

The Physical Origin of Scale Dependent Bias in Cosmological Simulations

Michael Blanton, Renyue Cen,
Jeremiah P. Ostriker, and Michael A. Strauss^{1,2}

Princeton University Observatory, Princeton, NJ 08544
blanton, cen, jpo, strauss@astro.princeton.edu

ABSTRACT

Using large-scale hydrodynamic simulations with heuristic criteria for galaxy formation, we investigate how the galaxy field is related to physical parameters, such as the mass density and the gas temperature. We find that the relation between the galaxy and mass density fields is a function of scale. The bias $b(R) \equiv \sigma_g(R)/\sigma(R)$, where $\sigma_g(R)$ is the variance of galaxy counts in spheres of radius R and $\sigma(R)$ is the same for mass, varies from 2.6 at $1 h^{-1}$ Mpc to 1.2 at $30 h^{-1}$ Mpc. Including the dependence of the galaxy density on local gas temperature as well as on local mass density can fully account for this scale dependence. Galaxy density depends on temperature because gas which is too hot cannot cool to form galaxies; this causes scale dependence of $b(R)$ because local gas temperature is related to the gravitational potential, and thus contains information about the large scale density field. We show that temperature dependence generally causes $b(R)$ to vary on quasilinear and nonlinear scales, indicating that scale dependence of bias may be a generic effect in realistic galaxy formation scenarios. We find that the relationship between the galaxy and mass density fields is also a function of galaxy age. On large scales, the older galaxies are highly biased ($b \approx 1.7$) and highly correlated ($r \equiv \langle \delta \delta_g \rangle / \sigma \sigma_g \approx 1.0$)

¹Alfred P. Sloan Foundation Fellow

²Cottrell Scholar of Research Corporation

with the mass density field; younger galaxies are not biased ($b \approx 0.8$) and are poorly correlated ($r \approx 0.5$) with the mass. We argue that linear bias is inadequate to describe the relationship between galaxies and mass. We present a more physically based prescription which better fits our results and reproduces the scale dependence of the bias: $\rho_g/\langle\rho_g\rangle = L(\rho/\langle\rho\rangle)^M(1 + T/40,000 \text{ K})^N$, where $L = 1.23$, $M = 1.9$, and $N = -0.66$.

Subject headings: large-scale structure of universe, galaxies: formation

1. Motivation

Imminent large-scale galaxy redshift surveys such as the Sloan Digital Sky Survey (SDSS; Gunn & Weinberg 1995) and the Two-Degree Field (2DF; Colless 1998) will probe the galaxy density field of the universe with unprecedented precision. Were galaxies accurate tracers of the mass density field, the results of these surveys would put severe constraints on cosmological models (de Laix & Starkman 1998; Tegmark *et al.* 1998; Goldberg & Strauss 1998; Wang, Spergel, & Strauss 1998). However, the visible matter in galaxies is only a small percentage of the baryons in the universe, which in turn is a small percentage of the mass in the universe (Fukugita, Hogan, & Peebles 1997; Cen & Ostriker 1998b). Moreover, the process of galaxy formation is complex and nonlinear, including a complicated interplay between gravitational fields, hydrodynamics, microphysics and star formation. Does this complicated process produce a population of galaxies whose number density field traces the mass density field perfectly? In this introductory section, we argue that observations already suggest not: that the relationship between the density fields of galaxies and mass is biased, scale dependent, and nonlinear, as well as dependent on morphological type. This discussion provides the observational motivation for asking the theoretical question: how is the galaxy density field related to that of the mass?

The crucial element of our argument is that different morphological types of galaxies have different density fields (Hubble 1936; Oemler 1974). Consider the observed differences between the clustering strengths of galaxies of different types. Various authors have compared elliptical and spiral galaxies, generally finding that the fluctuation amplitude of ellipticals is stronger than that of spirals by a factor of 1.3–1.5 (Davis & Geller 1976; Giovanelli, Haynes, & Chincarini 1986; Santiago & Strauss 1992; Loveday *et al.* 1996; Hermit *et al.* 1996; Guzzo *et al.* 1997). Similarly, a comparison of the galaxy distribution in the *IRAS* redshift survey (Strauss *et al.* 1992b) with those in the Center for Astrophysics Redshift Survey (CfA; Huchra *et al.* 1983) and in the Optical Redshift Survey (ORS;

Santiago *et al.* 1995), shows that optically-selected galaxies are clustered more strongly than infrared-selected galaxies by a similar factor (Davis *et al.* 1988; Babul & Postman 1990; Strauss *et al.* 1992a). These differences in the *amplitude* of clustering may be accounted for by invoking a deterministic linear bias prescription:

$$\delta_g(\mathbf{r}) = b \delta(\mathbf{r}), \quad (1)$$

where $\delta_g(\mathbf{r}) \equiv \rho_g(\mathbf{r})/\langle\rho_g\rangle - 1$ is the galaxy overdensity and $\delta(\mathbf{r}) \equiv \rho(\mathbf{r})/\langle\rho\rangle - 1$ is the mass overdensity, smoothed on some scale. To explain the observations, one must assume that different galaxy populations are “biased” by different factors b ; clearly at least one of these bias factors must differ from unity. Furthermore, there are differences between the shapes of correlation functions of galaxies of different types, at least at small scales. For instance, the ratio of the correlation functions of ellipticals and spirals found by Hermit *et al.* (1996) and Guzzo *et al.* (1997) declines with scale over the range between 1 and 10 h^{-1} Mpc. This scale dependence cannot result from a deterministic linear bias. Therefore, there must exist a more complicated relation between the density fields of different morphological types.

Alternatively, consider the density-morphology relation, quantified by Dressler (1980), Postman & Geller (1984), and Whitmore, Gilmore, & Jones (1993). In the field, spirals comprise about 70% of all galaxies, and ellipticals and lenticulars comprise the rest; in the cores of rich clusters the situation is reversed, and ellipticals and lenticulars account for 90% of all galaxies. Thus the overdensity of spirals as a function of the overdensity of all galaxies is highly nonlinear.

These differences among different morphological types suggest that the relationship between all galaxies and mass is comparably complicated. After all, it would be a coincidence if the overdensity field of all galaxies exactly traced the full mass overdensity, despite the fact that the different morphologies have formed at different times and with different efficiencies. In any case, the selection effects of redshift surveys (color, surface brightness, luminosity, *etc.*) will cause any catalog to contain a mix of morphological types that differs from the mix in the real universe. Since the overdensity fields of different morphologies have different density fields, the results of every survey are “biased” to some degree. It is thus interesting to explore theoretically how the mass density in the universe might be related to the galaxy density, and to the density of different morphological types.

One approach is to express the galaxy density as a local transformation of the dark matter density (or other variables), the simplest version of which is the deterministic linear bias of Equation (1). For instance, Fry & Gaztañaga (1993), Coles (1993), and Mann, Peacock, & Heavens (1997) have studied how nonlinear versions of this transformation can affect statistics such as the density distribution function, the correlation function, and M/L ratios of clusters. Another possibility is that the local transformation is not deterministic;

Scherrer & Weinberg (1997) show how such a stochastic relation affect the correlation function and the power spectrum of galaxies. Dekel & Lahav (1998) have developed a general formalism (which we adopt here) for expressing such a nonlinear and stochastic relation.

A second approach is to use semi-analytic models to simulate galaxy formation (Cole *et al.* 1994; Kauffmann *et al.* 1998; Somerville & Primack 1998). These methods use either N -body simulations or Press-Schechter (1974) analysis to follow dark matter halos and their merging histories, and use simple rules for star formation and feedback to follow the evolution of galaxies inside these halos. Kauffmann, Nusser, & Steinmetz (1997) and Kauffmann *et al.* (1998) used such models to study the relation between mass density and galaxy density. The third approach, which we adopt here, is to use hydrodynamic simulations with heuristic models of galaxy formation built into them. Generically, these simulations follow the radiative physics of the gas and use physically motivated prescriptions to convert baryonic fluid into collisionless stellar particles, which is necessary due to our ignorance of the details of the star-formation processes. Examples are Cen & Ostriker (1992b) and Katz, Hernquist, & Weinberg (1992, 1998).

In this paper, we examine the galaxy density field produced by the large-scale hydrodynamic simulations of Cen & Ostriker (1998a), which have sufficient dynamic range to examine the formation of galaxies in a cosmological context. In Section 2, we present the formalism of Dekel & Lahav (1998) for expressing the relation between galaxies and mass, and review some previous theoretical results. In Section 3, we present details of the numerical simulations of Cen & Ostriker (1998a). In Section 4, we examine the relation between the distributions of galaxies and mass in these simulations, as a function of smoothing scale and age. In Section 5, we show that one can explain the properties of the galaxy density field more completely by allowing for its dependence on gas temperature as well as on mass density. We present an analytic fit to our results which describes the galaxy density field well. In Section 6, we show that the dependence on gas temperature explains the scale dependence of the bias. Finally, we introduce a toy model which reproduces some of the salient properties of the galaxy density field, and shows how scale dependence could be a generic property of galaxy formation. We discuss some directions for future work in Section 7.

2. Formalism

In this section, we present a general formalism developed by Dekel & Lahav (1998) for expressing the present-day Eulerian relation between the galaxy and mass density fields

smoothed on a local scale R_0 . Such an approach, which considers only the density fields at $z = 0$, of course does not account for the fact that two regions which have similar properties now may have had significantly different histories. We relate this formalism to the simple approximation that the galaxy and mass densities form a bivariate Gaussian distribution. Finally, we describe how certain complications allowed by this formalism, namely nonlinearity and stochasticity, can cause the relation between the two density fields to be a function of scale.

We begin by defining $P(\delta_g|X_i)$ as the conditional probability of a certain overdensity of galaxies $\delta_g \equiv \rho_g/\langle\rho_g\rangle - 1$, given the set of *local* conditions expressed by X_i , where the X_i can be mass density, temperature, velocity shear, or any other present-day parameter thought to be relevant to galaxy formation. We use this probabilistic formalism despite the fact that galaxy formation is a deterministic process, for two reasons. First, two regions with the same galaxy density at $z = 0$ may have had quite different histories; these differences may make it impossible to find a perfectly deterministic relation between δ_g and other Eulerian variables. Second, even if such a relation did exist, one might not be able to identify the correct set of Eulerian variables with which to express it. Choosing a wrong or incomplete set of X_i would cause the relation to have large scatter. Because this resulting “stochasticity” would in fact have a physical basis, it would be likely to have statistical properties that differed from those of a truly random variable. Thus, one of our goals will be to find a set of X_i which minimizes this scatter.

Having defined the conditional probability, one can define the conditional mean:

$$\langle\delta_g|X_i\rangle \equiv \int d\delta_g \delta_g P(\delta_g|X_i). \quad (2)$$

The variance of the scatter about this mean is:

$$\sigma_b^2 \equiv \langle\epsilon^2\rangle = \langle(\delta_g - \langle\delta_g|X_i\rangle)^2\rangle, \quad (3)$$

where, as indicated, ϵ represents the residuals of the conditional mean galaxy density at scale R_0 . The quantity σ_b/σ_g , where $\sigma_g^2 \equiv \langle\delta_g^2\rangle$, expresses the degree of stochasticity in the relation between galaxies and the variables X_i . Typically, investigators in this field have assumed that the most important (if not the only) local condition worth considering is the mass overdensity $X_i = \delta \equiv \rho/\langle\rho\rangle - 1$ (an exception being Weinberg 1995). In this case, one considers the conditional probability $P(\delta_g|\delta)$ and the corresponding conditional mean $\langle\delta_g|\delta\rangle$, which is meant to summarize the relation between galaxies and mass on the given scale R_0 .

If the joint distribution of δ and δ_g is a bivariate Gaussian at scale R_0 , which is close

to being true in the linear regime, the joint probability can be expressed as:

$$P(\delta, \delta_g) = \frac{1}{2\pi\sqrt{\sigma^2\sigma_g^2 - \langle\delta\delta_g\rangle^2}} \exp\left(-\frac{1}{2}\frac{\sigma_g^2\delta^2 - 2\langle\delta\delta_g\rangle\delta\delta_g + \sigma^2\delta_g^2}{\sigma^2\sigma_g^2 - \langle\delta\delta_g\rangle^2}\right). \quad (4)$$

We will refer to this special case as “linear bias.” Such a distribution can be characterized by three quantities: $\sigma^2 \equiv \langle\delta^2\rangle$, $b \equiv \sigma_g/\sigma$, and $r \equiv \langle\delta\delta_g\rangle/\sigma\sigma_g$, and indeed, this motivates the definitions of these quantities for arbitrary $P(\delta, \delta_g)$. In the rest of this paper we will refer to b as the “bias” and r as the “correlation coefficient.” The bias compares the r.m.s. amplitude of the galaxy overdensity to that of the mass overdensity. The correlation coefficient expresses how closely the galaxy density field traces the mass density field. That is, if $r = \pm 1$, the relation between mass and galaxies is deterministic; if $r = 0$ the galaxies are distributed independently of the mass. Note that the Gaussian assumption implies:

$$\begin{aligned} \langle\delta_g|\delta\rangle &= br\delta; \\ \sigma_b/\sigma_g &= \sqrt{1-r^2} \quad (\text{Gaussian model}). \end{aligned} \quad (5)$$

In the nonlinear regime, the density field is far from Gaussian; however, calculating the second moments b and r will still give useful information on how the galaxy and mass density fields relate. The quantity br for any given pair of galaxy and mass density fields is the slope of a linear regression of δ_g on δ . Similarly, b/r is the slope of the linear regression of δ on δ_g . The quantity $\sqrt{1-r^2}$ is a measure of the scatter around either regression. The scatter can occur either because nonlinearities make a straight line a poor approximation to $\langle\delta_g|\delta\rangle$, or because of stochasticity. As Dekel & Lahav (1998) note, the ratio $\sigma_b/(\sigma_g\sqrt{1-r^2})$ measures the contribution of stochasticity (as opposed to nonlinearity) to the total scatter around the linear regression br .

In the context of the formalism presented here, let us examine how scale dependence in the relation between galaxies and mass may arise. The most common assumption about bias in studies of large-scale structure is that the deterministic linear bias of Equation (1) holds (*i.e.* $r = 1$). Such a relation is scale independent; the same factor b applies at all scales. However, $\langle\delta_g|\delta\rangle$ may in general be a nonlinear function of δ . In fact, on scales at which $\sigma \gg 1$, this nonlinearity inevitably results from the condition $\delta_g > -1$ (as long as $\langle\delta_g|\delta\rangle$ does not *exactly* equal δ). A simple approach is to expand δ_g in a Taylor series around δ (Fry & Gaztañaga 1993):

$$\langle\delta_g|\delta\rangle = b_1\delta + \frac{b_2}{2}(\delta^2 - \langle\delta^2\rangle) + \frac{b_3}{6}(\delta^3 - \langle\delta^3\rangle) + \dots \quad (6)$$

The introduction of nonlinearity opens the door to scale dependence; if δ_g and δ are smoothed on a scale above R_0 , the coefficients in Equation (6) may change. On the other

hand, Scherrer & Weinberg (1997) show that even in the presence of nonlinear bias on small scales of the form in Equation (6), $b(R)$ is independent of R on large scales (at least under the assumption of hierarchical clustering).

In addition to being nonlinear, the relation can be stochastic, such that $\sigma_b \neq 0$. Scherrer & Weinberg (1997) have examined $b(R)$ in this case as well, and concluded that it could not be a function of scale. However, they assumed that the residual field ϵ about $\langle \delta_g | \delta \rangle$ is purely random. On the other hand, we said earlier that the scatter ϵ probably has a physical basis; thus, it is possible that ϵ correlates with the large scale density field. If such a correlation existed, $b(R)$ would be a function of scale. To illustrate this possibility, assume for the moment that at some small smoothing scale R_0 , the joint δ_g - δ distribution is a bivariate Gaussian, with a bias of $b(R_0)$ and correlation coefficient $r(R_0)$. We define $\epsilon \equiv \delta_g - br\delta$ on this scale. We can subsequently smooth δ_g , δ , and ϵ over a large scale $R \gg R_0$. In this case:

$$b^2(R) = b^2(R_0)r^2(R_0) + \frac{\langle \epsilon^2 \rangle_R + 2b(R_0)r(R_0)\langle \delta\epsilon \rangle_R}{\sigma^2(R)}. \quad (7)$$

As $R \rightarrow R_0$, by definition we have $\langle \delta\epsilon \rangle_R \approx 0$ and $\langle \epsilon^2 \rangle_R \approx \sigma_g^2(R_0)(1 - r^2(R_0))$, so that $b(R \rightarrow R_0) = b(R_0)$ as necessary. If $\langle \delta\epsilon \rangle_R$ or $\langle \epsilon^2 \rangle_R$ varies on larger scales, clearly $b(R)$ will vary as well. We show below that this variation can result from fairly simple physical considerations; indeed, the effects are strong in the simulations considered here.

In the following sections, we will describe the numerical simulations of Cen & Ostriker (1998a) and present the results in the context of the formalism presented here. As the independent variable X_i , we at first use the traditional dark matter overdensity δ , and find that the dependence on δ cannot completely characterize the galaxy density field. We will find that using the description $P(\delta_g | \delta, T)$, where T is the local gas temperature, gives a much more satisfactory description of the galaxy density field. In particular, accounting for the dependence on T (or its counterpart, the dark matter velocity dispersion $\langle v^2 \rangle$) also accounts for most of the scale dependence of the bias. Thus, temperature dependence causes stochasticity in the galaxy-mass relation, and this stochasticity is correlated with the mass distribution over large scales, causing $b(R)$ to vary with scale.

3. Simulations

For these simulations, the work of Ostriker & Steinhardt (1995) motivated the choice of a flat cold dark matter cosmology with $\Omega_0 = 0.37$, $\Omega_\Lambda = 0.63$, and $\Omega_b = 0.049$. The Hubble constant was set to $H_0 = 100 h \text{ km s}^{-1} \text{ Mpc}^{-1}$, with $h = 0.7$. The primordial perturbations

were adiabatic and random phase, with a power spectrum slope of $n = 0.95$ and amplitudes such that $\sigma_8 = 0.8$ for the dark matter at $z = 0$, at which time the age of the universe is 12.7 Gyrs. We use a periodic box $100 h^{-1}$ Mpc on a side, with 512^3 grid cells and 256^3 dark matter particles. Thus, the mass resolution is about $5 \times 10^9 M_\odot$ and the grid cell size is $\sim 200 h^{-1}$ kpc. The smallest smoothing length we consider is a $1 h^{-1}$ Mpc radius top hat, which is considerably larger than a cell size; thus, our results are relatively insensitive to the code resolution.

Cen & Ostriker (1998a) describe the hydrodynamic code in detail; it is similar to but greatly improved over that of Cen & Ostriker (1992a). The simulations are Eulerian on a Cartesian grid and use the Total Variation Diminishing method with a shock-capturing scheme. In addition, the code accounts for cooling processes and incorporates a heuristic galaxy formation criterion, whose essence is as follows: if a cell’s density is high enough, if the cooling time of the gas in it is shorter than its dynamical time, if it contains greater than the Jeans mass, and if the flow around that cell is converging, it will have stars forming inside of it. The code turns a fraction of the baryonic fluid component into collisionless stellar particles (hereafter “galaxy particles”), which subsequently contribute to metal production and the background ionizing UV radiation. The masses of these galaxy particles range from about 10^6 to $10^9 M_\odot$. Thus, many galaxy particles are contained in what would correspond to a single galaxy in the real universe. Instead of grouping the particles into galaxies, we simply define a galaxy mass density field from the distribution of galaxy particles themselves.

We are interested in examining the dependence of the galaxy density field on galaxy morphology, to explore the differences between different galaxy types noted in Section 1. The simulations do not have sufficient resolution to resolve structure in individual galaxies; however, they do keep track of the age of each galaxy particle. Since the morphology of galaxies appears to be related to their star formation history, we use age as a rough proxy for morphology. Therefore, we can examine the simulations for an age-density relation corresponding to the morphology-density relation of Dressler (1980) and Postman & Geller (1984). Cen & Ostriker (1993) did so, finding qualitatively that the oldest galaxies had fallen into clusters and that the younger galaxies were forming in the lower density regions. In addition, Cen & Ostriker (1998a) have examined the dependence of the power spectrum on galaxy age. Here, we visit the problem again, by splitting the galaxy particles into four age quartiles, defined such that the total mass of galaxy particles in each quartile is the same. The age and redshift ranges of the quartiles are given in Table 1. As we examine the properties of the full galaxy mass density field, we do the same for the density fields of each age quartile.

Figures 1a and 1b show a slice through the galaxy and dark matter density fields $50 h^{-1}$ Mpc on a side, at $1 h^{-1}$ Mpc and $10 h^{-1}$ Mpc smoothing, respectively. From top left, in clockwise order, we show the quantity δ for the dark matter, all of the galaxy particles, the youngest galaxy quartile, and the oldest galaxy quartile. For each of these, δ is normalized to the mean density of the sample in question, so that in the absence of biasing, these plots would be identical. Evidently the galaxy distribution follows the dark matter distribution well, except in the underdense regions, which are completely empty voids in the galaxy particle distribution. It is apparent from these pictures that the youngest galaxy particles are distributed quite differently than is the mass. At small smoothing scales the effect is obvious only in the clusters; otherwise the young galaxies follow the dark matter. At large smoothing scales, however, the young galaxies are underdense in the clusters, and their density fields peak along the filaments. On the other hand, the oldest galaxies follow the mass distribution well on all scales, and are quite obviously biased. In the rest of the paper, we will quantify the differences among these various density fields.

4. Single-Variable Bias

In this section, we study the relation between the galaxy and mass density fields, expressed by $P(\delta_g|\delta)$ and $\langle\delta_g|\delta\rangle$. We begin by smoothing the galaxy density field over several different scales and showing that the relationship between galaxies and mass is a function of scale. Then we show that it is the properties of the scatter about $\langle\delta_g|\delta\rangle$ at small scales, and not the form of $\langle\delta_g|\delta\rangle$ itself, which causes this scale dependence.

4.1. Galaxy Density vs. Mass Density

First we directly compare the density field of dark matter to that of galaxies. We do so by plotting in Figure 2 the conditional probability $P(1 + \delta_g|1 + \delta)$ using top hat smoothing filters of six different radii: 1, 2, 5, 8, 16, and $30 h^{-1}$ Mpc. We use $1 + \delta$ here simply for convenience in plotting the results. The greyscale in this figure is a logarithmic stretch of $P(1 + \delta_g|1 + \delta)$; the greyscale for each column is normalized separately. Note that for small smoothing scales, the discreteness of the dark matter particles limits our measurement of δ in voids. The vertical dashed line is the density corresponding to about 50 particles within one smoothing length, below which this effect becomes important. Note further that there is structure in the histograms at large smoothing scales, since there are many bins in the histogram but only a few truly independent values in the periodic volume. We plot $\langle\delta_g|\delta\rangle$ for each smoothing scale as the solid black lines; the 1σ deviations from this mean line are

shown as the dotted black lines. It is immediately apparent that this function is nonlinear, and that there is large scatter about it.

The same comparison can be made for the galaxies in each age quartile separately, as is shown in Figures 3a and 3b for top hat smoothing filters of two radii: 1 and 30 h^{-1} Mpc. The overdensity δ_g for each quartile is defined by normalizing to the mean density of that quartile. Note that there is a tight and highly biased relation between the distributions of older galaxies and the dark matter. On the other hand, the relation between the youngest galaxies and the mass is quite stochastic, even at the largest scales. At small scales, $\langle\delta_g|\delta\rangle$ for young galaxies is not monotonic; as in the real universe, young galaxies rarely live in the highest density regions. This trend with age is easily understood. The densest regions of the universe are in the deepest potential wells, so they have the hottest gas with the longest cooling times; thus, this gas stopped forming galaxies some time ago. As a consequence, on average, the galaxies in the densest regions are older than galaxies elsewhere.

One can quantify the relation between galaxies and mass by calculating second moments of the galaxy-mass distribution. Thus, at each smoothing scale, we calculate the parameters $b \equiv \sigma_g/\sigma$ and $r \equiv \langle\delta_g\delta\rangle/\sigma_g\sigma$ and list their values in Table 2. Note that b declines strongly with scale, from 2.6 at 1 h^{-1} Mpc to 1.2 at 30 h^{-1} Mpc; this behavior is consistent with the work of Cen & Ostriker (1992b). Meanwhile, $r \sim 0.9$ almost independent of scale, meaning that galaxies are well-correlated with mass. Similarly, we can calculate σ_b , the variance of the scatter about $\langle\delta_g|\delta\rangle$, and find that $\sigma_b/\sigma_g \sim 0.3$ – 0.4 . For comparison to r , we list the ratio $\sigma_b/\sigma_g\sqrt{1-r^2}$, which is ~ 0.8 – 0.9 at all scales, indicating that stochasticity, rather than nonlinearity, dominates the scatter around the linear regression slopes br and b/r .

The parameters b and r will also clearly depend on what age galaxies one considers, as Figures 3a and 3b indicate. In Table 3 we list b and r for each of the quartiles and smoothing scales used in Figures 3a and 3b. Again, the dependence on scale is evident. However, more prominent are the differences between galaxies of different ages. Older galaxies are much more highly biased than young galaxies at all scales. In addition, older galaxies are more correlated with the mass distribution; $r \sim 0.9$ – 1.0 for the oldest galaxies, while $r \sim 0.5$ for the youngest galaxies. These results agree with observations that early-type galaxies are biased relative to late-type galaxies. The low correlation coefficient for young galaxy particles means that fluctuations in their density field are poorly correlated with fluctuations in the mass density field, as one can see from Figures 1a and especially 1b; that b is near unity on large scales merely indicates that the fluctuations in the two fields are of similar amplitudes.

4.2. Scale Dependence

To study more carefully the scale dependence of the bias, we show $b(R)$ in Figure 4 and $r(R)$ in Figure 5. The solid black lines refer to all the galaxies; the dashed lines refer to each age quartile, as labeled. These curves show the same behavior found in Tables 2 and 3. The older galaxies are more biased than the younger galaxies. Furthermore, the density field of the oldest quartile is extremely well-correlated with the mass density field, while that of the youngest quartile is extremely poorly correlated. Meanwhile, bias declines with scale for all the galaxies and for each quartile. This scale dependence can be due to two things only: the nonlinearity of the locally defined $\langle\delta_g|\delta\rangle$, or the properties of the field of residuals ϵ about that mean.

Several theoretical forays suggest that the first possibility cannot be the case (Coles 1993; Scherrer & Weinberg 1997; Dekel & Lahav 1998). We can test these results by applying the $\langle\delta_g|\delta\rangle$ defined on small scales to the mass density field. Specifically, we calculate $\langle\delta_g|\delta\rangle$ for the galaxy and mass fields smoothed with a $1 h^{-1}$ Mpc radius top hat; then, at each grid cell, we check the value of δ and set the galaxy density in that cell to the appropriate value of $\langle\delta_g|\delta\rangle$. We refer to the resulting field as the “fake galaxy” density field.

We can now consider the statistic $b(R)$ for this fake galaxy field, which we determined using the mass density field alone, shown as the dotted lines in each panel of Figure 6. Here, R takes into account the $1 h^{-1}$ Mpc smoothing already present in δ . The solid lines are the actual $b(R)$ for the galaxies found in the simulations, from Figure 4. The top panel corresponds to all the galaxies, the middle panel to the oldest galaxies, and the bottom panel to the youngest galaxies. One can see that this fake bias procedure does not reproduce the behavior of bias as a function of scale, at least when we use this single-variable model $\langle\delta_g|\delta\rangle$. At small scales, the “fake” galaxy distribution has less power than the actual galaxy distribution, partly due to the fact that the fake galaxy distribution is a deterministic function of the underlying dark matter density. There is some scale dependence, which is allowed by the results of Scherrer & Weinberg (1997) in the nonlinear regime. However, at large scales, the fake galaxy distribution remains much more biased than the actual galaxy distribution. Thus, not all the information about the galaxy density field is contained in the mean relation $\langle\delta_g|\delta\rangle$ between galaxies and mass at small scales.

The remaining possibility is that the properties of the residual field ϵ about $\langle\delta_g|\delta\rangle$ cause the scale dependence. These residuals must correlate over large scales in such a way that $\epsilon < 0$ in large scale overdensities and $\epsilon > 0$ in large scale voids. In that case, $\langle\delta\epsilon\rangle_R$ will be negative on large scales and, as Equation (7) reveals, $b(R)$ will decrease with scale. To test this possibility, we calculate ϵ at $1 h^{-1}$ Mpc top hat smoothing, and then smooth ϵ and δ on scale R in order to calculate $\langle\delta\epsilon\rangle_R/\sigma^2(R)$. Figure 7 shows the behavior of this

quantity. As one would predict, it is near zero when $R \sim 1 \ h^{-1}$ Mpc, and becomes strongly negative on larger scales. The same holds for the youngest and oldest quartiles, also shown in Figure 7. This result indicates that, indeed, the residual field tends to be negative in large scale overdensities, and positive in large scale voids.

In other words, the scatter about $\langle \delta_g | \delta \rangle$ is far from purely random. It depends on other variables which are important to galaxy formation. The dependence on and the nature of these variables must be such as to reproduce the scale dependence found in this section. In the next two sections, we investigate the dependence of galaxy density on a number of other variables, and find that accounting for the dependence of galaxy density on local temperature can both reduce the scatter in the residual field and explain the scale dependence of b .

5. Two-Variable Bias

From the last section we learned that modeling the galaxy density field as a function of mass density alone was unsatisfactory. We would like to both reduce the stochasticity in our estimate of the galaxy density and to explain the scale dependence of $b(R)$. To do so, we can add an independent variable to our conditional probability and consider the function $P(\delta_g | \delta, X_i)$. We try several X_i and find that the most successful is the local gas temperature T , or, equivalently, the local dark matter velocity dispersion. This result is perhaps not surprising, since gas temperature is surely an important parameter in galaxy formation. In addition, we find in Section 6 that accounting for this dependence on T also accounts for the dependence of $b(R)$ on scale.

For each X_i we choose as a second independent variable, we want to know how much it reduces the stochasticity in the relation $P(\delta_g | \delta, X_i)$. To quantify this, we calculate the ratio:

$$\frac{\sigma_{b,2}}{\sigma_b} = \frac{\langle (\delta_g - \langle \delta_g | \delta, X_i \rangle)^2 \rangle^{1/2}}{\langle (\delta_g - \langle \delta_g | \delta \rangle)^2 \rangle^{1/2}}, \quad (8)$$

which expresses the scatter of δ_g around $\langle \delta_g | \delta, X_i \rangle$, compared with the scatter around $\langle \delta_g | \delta \rangle$. Thus, if X_i is perfectly correlated with δ , or if it is perfectly uncorrelated with δ_g , then $\sigma_{b,2}/\sigma_b \approx 1$. In the next few paragraphs, we will substitute for the variable X_i the following: T , the local temperature; $\langle v^2 \rangle$, the local dark matter velocity dispersion; the prolateness and oblateness of the local dark matter density field; and the shear in the dark matter velocity field. Our results for $\sigma_{b,2}/\sigma_b$ for these variables are given in Table 4.

The local temperature T is relevant to galaxy formation because gas which is too hot cannot cool and form stars. Figure 8 shows a contour plot of galaxy density as a function of

mass density and gas temperature; all fields in this plot have been smoothed over $1 h^{-1}$ Mpc radius top hat spheres. First, note that local gas temperature and local dark matter density are clearly not independent variables; the upper left triangle in the figure is blank because there are no volume elements with high local density and low temperature on these scales. Nevertheless, one can see that galaxy density declines at constant δ as the temperature increases. Figure 9 shows δ_g as a function of T for $\delta = 20$, corresponding to a horizontal slice of Figure 8. The strength of the temperature dependence is evident. From Table 4, we note that the inclusion of this extra variable reduced the variance by over a factor of two, indicating that variations in local temperature can account for a large portion of the stochasticity in the biasing relations of Figure 2. In Figure 9 we also plot the dependence on temperature of the galaxy density in each age quartile, as the dashed curves. As one would expect, the density of the youngest galaxies is the most temperature-dependent; that is, in the hottest regions, there are no new galaxies forming, although plenty of old galaxies exist there, which formed there in the past or have since fallen in.

A fairly good fit to the dependence of galaxy density on mass density and temperature on small scales is:

$$\frac{\rho_g}{\langle \rho_g \rangle} = L \left(\frac{\rho}{\langle \rho \rangle} \right)^M \left(1 + \frac{T}{40,000 \text{ K}} \right)^N. \quad (9)$$

We show such a fit in Figure 10. As labeled, each pair of solid and dotted lines corresponds to a different value of δ . The solid lines are the results from Figure 8; the dotted lines are the fit of Equation (9), using $L = 1.23$, $M = 1.9$, and $N = -0.66$. For $N < 0$, the factor involving T takes into account the fact that relatively fewer galaxies have formed in hotter regions; the form assumed here reflects the approximate power law dependence in Figures 9 and 10. This effect is not important once the gas is as cold as 40,000 K, and thus we construct the temperature factor to have no effect in that regime.

We would like to be able to apply such a fit to N -body simulations. Doing so would allow us to explore changes of cosmological parameters more easily than the expensive hydrodynamical simulations allow. Although we cannot follow gas temperature in purely collisionless simulations, we can calculate the related quantity $\langle v^2 \rangle$, the local dark matter velocity dispersion. The dependence on $\langle v^2 \rangle$ should be similar to that on local gas temperature. After all, in virialized regions the velocity dispersion of dark matter particles cannot differ wildly from the velocity dispersion of individual atoms. Indeed, from Table 4 it is clear that $\sigma_{b,2}/\sigma_b$ is nearly the same for the velocity dispersion as it is for the temperature. Note, of course, that taking into account the dependence of galaxy density on *both* $\langle v^2 \rangle$ and T would not improve on using either one separately, as they are essentially equivalent variables.

Next, we consider the oblateness and prolateness of the density field in spheres of $1h^{-1}$ Mpc, calculated from the eigenvalues of the local inertia tensor $\lambda_1, \lambda_2, \lambda_3$; the prolateness is $2\lambda_1/(\lambda_2 + \lambda_3) - 1$ and the oblateness is $(\lambda_1 + \lambda_2)/2\lambda_3 - 1$. As one can see from Table 4, these quantities are not important to the galaxy density. Finally, we consider the shear in the velocity field, defined by:

$$\begin{aligned}\Sigma^2 &= \sum_{ij} (\Sigma_{ij})^2, \text{ where} \\ \Sigma_{ij} &= \frac{1}{2}(v_{i,j} + v_{j,i}) - \frac{1}{3}v_{k,k}\delta_{ij}.\end{aligned}\tag{10}$$

Clearly the shear will correlate well with the dark matter density, as the dark matter in the higher density regions will have higher velocities. To account for this, we consider the dimensionless quantity $\Sigma^2/H_0^2(1 + \delta)$. Another way to justify this scaling is to think of the Σ as a characteristic shearing rate, to be multiplied by the dynamical time, which scales as $(1 + \delta)^{-1/2}$. From Table 4, the galaxy density seems largely independent of the shear in the velocity field. Thus temperature, or equivalently velocity dispersion, seems to be the relevant second parameter for the dispersion relation. Of course, the parameters considered here do not by any means exhaust the list of properties of possible importance to galaxy formation.

6. Explaining Scale Dependence

The last section revealed that local temperature is an important parameter for determining the local galaxy density. Is it possible that the temperature dependence can affect the scale dependence of $b(R)$? We can repeat the exercise of Section 4 and calculate a fake galaxy density field, this time using the two-variable mean $\langle \delta_g | \delta, T \rangle$ of Figure 8. We then calculate $b(R)$ as before and plot it as the short dashed line in each panel of Figure 6. The temperature dependence indeed beautifully accounts for the variation of $b(R)$ with scale, for all the galaxies as well as for each quartile. The fit to the density distribution given by Equation (9) produces nearly identical results; it is shown as the long dashed line in the upper panel.

What are the physical properties of the temperature field that cause this to happen? Essentially, it is that local temperature reflects the gravitational potential and thus contains information about the large scale density field. The temperature fluctuations $\delta_T \equiv T/\langle T \rangle - 1$ can be expressed in a simple way by considering some limits (Spergel 1998). First, in the nonlinear regions, gas is virialized and its temperature must scale as the local potential. From Poisson’s equation, one knows that $\tilde{\phi}(\mathbf{k}) \propto k^{-2}\tilde{\delta}(\mathbf{k})$. Thus, on small scales, it must be

that $\tilde{\delta}_T(\mathbf{k}) \propto k^{-2}\tilde{\delta}(\mathbf{k})$ as well. Second, on linear scales one can assume that the temperature fluctuations are dominated by the number density fluctuations of virialized haloes, since gas in those areas is much hotter than that in the empty regions between halos. Thus, on large scales $\tilde{\delta}_T(\mathbf{k}) \propto \tilde{\delta}(\mathbf{k})$. These two limits may be combined:

$$\tilde{\delta}_T(\mathbf{k}) \propto \frac{\tilde{\delta}(\mathbf{k})}{1 + k^2 r_{nl}^2 / (2\pi)^2}, \quad (11)$$

where r_{nl} is the transition scale between the linear and nonlinear regimes. Consequently, we expect the cross spectrum of temperature and mass to be:

$$P_{Tm}(k) \propto \frac{P_{mm}(k)}{1 + k^2 r_{nl}^2 / (2\pi)^2}. \quad (12)$$

In Figure 11, we compare this simple model with the simulations, finding that it is a good fit for the choice $r_{nl} = 16 \ h^{-1}$ Mpc. This value for r_{nl} agrees approximately with the scale on which nonlinear effects should become important. Thus, the temperature power spectrum peaks at large scales; furthermore, at those scales the temperature fluctuations are directly related to the mass density. That means that the largest contribution to the local temperature actually comes from large wavelength fluctuations, which follow the large wavelength fluctuations in mass density. The local gas temperature is therefore a direct indicator of the large scale density field. Thus, accounting for the temperature dependence automatically accounts for the dependence on large scale density, and consequently the dependence of bias on scale.

A simple model for the relation between galaxies, mass, and temperature reveals more explicitly how scale dependence and stochasticity enter the relation between galaxies and mass. Consider the fit given in Equation (9). If one assumes that $\delta_g \ll 1$, $\delta \ll 1$, and $\delta_T \ll 1$, this relation becomes:

$$\delta_g = M'\delta + N'\delta_T, \quad (13)$$

and one recovers the deterministic linear bias model if $N' = 0$ and $M' = b$. This model is obviously highly unrealistic, especially at small scales. However, its simplicity will allow us to understand better how $b(R)$ becomes scale-dependent.

We can perform a linear regression on δ and δ_T to determine M' and N' . The results as a function of top hat smoothing scale are shown in Figure 12. Notice that M' and N' are approximately constant with respect to scale. This invariance indicates that the scale dependence is well-accounted for by the temperature dependence. To examine this claim, let us assume that Equation (13) holds at some small scale R_0 . Now, if we smooth over a larger scale R , we find that:

$$b^2(R) \equiv \frac{\sigma_g^2(R)}{\sigma^2(R)} = M'^2 + N'^2 \frac{\sigma_T^2(R)}{\sigma^2(R)} + 2M'N' \frac{\langle \delta \delta_T \rangle_R}{\sigma^2(R)}. \quad (14)$$

Note that $\langle \delta \delta_T \rangle_R / \sigma^2(R)$ and $\sigma_T^2(R) / \sigma^2(R)$ will depend on R , because Equation (11) shows that $P_{Tm}(k) / P_{mm}(k)$ and $P_{TT}(k) / P_{mm}(k)$ depend on k . Thus, $b(R) \equiv \sigma_g(R) / \sigma(R)$ will also depend on R . We can test this possibility directly by applying the deterministic two-variable linear model to this simulation and calculating $b(R)$. For this test we use the values $M' = 2.4$ and $N' = -0.4$, which are appropriate at $1 h^{-1}$ Mpc; the resulting curve is the dot-dashed line in the upper panel of Figure 6. At small scales, the linear approximation is (as expected) poor but of the right order; on large scales, it reproduces the value of $b(R)$ fairly well.

Thus, even this simple linear model reproduces the scale dependence. We do not claim that this model is a particularly *good* one for describing the galaxy density; the fit of Equation (9) is much better. Instead, the linear model is merely a toy which illustrates the following point: given a dependence of galaxy density on local temperature, it is inevitable that $b(R)$ is a function of scale on scales smaller than about r_{nl} , simply because of the relationship between gas temperature and mass density.

7. Discussion

Consider two regions of the universe, both of which have the same local mass overdensity; however, with respect to the large scale density field, one is in an overdensity, the other in a void. The gas in these two regions will evolve similarly, forming galaxies with about equal efficiency, until the large scale density field becomes nonlinear. At this point, the ambient gas around the first region, in the large scale overdensity, will become too hot to accrete any longer, and galaxy formation will cease. Meanwhile, the gas around the second region, in the void, will remain cool enough to accrete onto old galaxies and continue to form new ones. This picture explains part of the scatter in the local relation between δ and δ_g ; it also explains why this scatter is such that in hot regions $\epsilon \equiv \delta_g - \langle \delta_g | \delta \rangle < 0$, and in cold regions $\epsilon > 0$. In turn, the correlation of temperature with large scale density explains why ϵ also correlates with large scale density, causing scale dependent bias. In addition, it indicates qualitatively why spirals, which are caused by late-time accretion of gas, are relatively more abundant in the “field” and relatively underabundant in the rich clusters.

In this scenario, scale dependent bias follows from only one rather robust assumption: that the ambient gas temperature affects the efficiency of galaxy formation. Since gas must be able to cool to form galaxies, this assumption is well-motivated theoretically. Furthermore, observations of the star-formation rate as a function of local density indicate that, indeed, star formation is reduced in the hot cluster environments, even at a fixed

morphological type (Young *et al.* 1996; Hashimoto *et al.* 1997; Balogh *et al.* 1998). Once one concedes that local temperature is an indicator of the how efficient galaxy formation has been, the arguments in Section 6 lead one to directly conclude that $b(R)$ should depend on scale, at least in the quasilinear and nonlinear regimes, where $P_{Tm}(k)$ and $P_{TT}(k)$ have different shapes than $P_{mm}(k)$. In the simulations studied here, the effects are particularly strong.

Scale dependence in the relation between galaxies and mass can affect the interpretation of future redshift and peculiar velocity surveys. The most obvious example is that on small scales, the shape of the galaxy power spectrum will differ from that of the mass. Furthermore, as pointed out by Dekel & Lahav (1998), comparison of the observed galaxy density field to that inferred from observed peculiar velocities (Dekel 1994; Sigad *et al.* 1998) effectively perform a regression of δ on δ_g and thus measure the quantity $\beta = (r/b)f(\Omega)$, which we show here depends both on scale and on the chosen galaxy sample. Thus, the current analyses, usually performed in the quasilinear regime and using *IRAS* galaxies³ to define the density field, may be sensitive to these effects. For instance, one’s estimate of r/b will generally increase with scale, by about 20% between $5 h^{-1}$ Mpc and $30 h^{-1}$ Mpc. Amusingly, although r and b vary by a factor of two between the youngest and oldest galaxies on large scales, the dependence of r/b on galaxy age remains quite small; $r/b \sim 0.6$ – 0.7 for all four quartiles. In the real world, the regression of δ on δ_g will most likely not be this constant among the morphological types. The decrease of β with scale could contribute to the differences between the results of Sigad *et al.* 1998 and of analyses carried out with smaller smoothing scale, such as VELMOD (Willick & Strauss 1998); however, there are stark differences between these methods, and a more careful analysis is thus necessary. Indeed, we are interested in exploring the effects of the nonlinear stochastic bias we are seeing on a variety of large-scale structure statistics inferred from redshift surveys, including redshift-space distortions (Dekel & Lahav 1998) and the pairwise velocity dispersion as a function of local density (Strauss, Ostriker & Cen 1998). A full treatment will require identifying individual galaxies from the galaxy particles in the simulations, which will require tackling the overmerging problem in the densest regions of the simulations.

We can address some of these issues without having to run expensive hydrodynamic simulations for a range of cosmological models. First, in order to examine in detail the

³*IRAS* galaxies are typically young, although they are probably not as young as our youngest quartile. In particular, *IRAS* galaxies do not show an underdensity in rich clusters that the youngest galaxies in the simulations do (Fig. 1b), although they are less overdense than optically selected galaxies (Strauss *et al.* 1992a).

effect of the relation between galaxy density, mass density, and temperature on all of these statistics, we plan to carry out N -body simulations of larger dynamic range than is possible with the current hydrodynamical simulations. To characterize the galaxy distribution in these simulations, we will apply the model of Equation (9), using $\langle v^2 \rangle$ as a proxy for temperature. Then one can explore the effect this type of bias can have on the various statistics discussed in the last paragraph. A second approach is to analyze observations, allowing for scale dependent bias of the character described here. In this vein, one could investigate the differences between galaxy types and see how they compare in detail with the differences we find between our age quartiles. Most interestingly, one could try to make consistent the divergent observed values of β (Strauss & Willick 1995).

Of course, that temperature is the important *causal* variable in these simulations is based only on a *post hoc* (though physically plausible) argument. Any variable that probes the large-scale density field would serve just as well to reduce $\sigma_{b,2}/\sigma_b$ and explain the scale dependence of $b(R)$. However, as discussed above, temperature is a well-motivated quantity. Controlled tests of the effect of ambient temperature on star formation in these simulations might help clarify the matter. Another approach is to look at various output times and examine under what conditions in the simulations the galaxies actually form. We plan to do so in a future paper, which will examine the history of galaxy formation and bias in these simulations.

The alert reader will notice that some of our results contradict our opening statements in Section 1. In particular, if one looks at our results on large scales, it does happen to be true that the distributions of old galaxies and of young galaxies both differ considerably from the mass distribution, but in combination trace the mass quite well and are almost unbiased. We simply note here that the same would not be true were we to look at the results of these simulations at $z = 0.5$, for instance. In addition, Cen & Ostriker (1992b) found that for a hot dark matter universe (HDM), b was significantly greater than unity on large scales, indicating that the level of bias in these simulations depends somewhat on the chosen cosmology. Thus we ascribe little importance to this coincidence in the current simulations. In any case, we plan further investigations to investigate the redshift dependence of the bias, following the predictions of Fry (1996) and Tegmark & Peebles (1998).

Several more notes of caution are in order concerning applying these results in detail. First, the simulations have limited resolution and do not probe physics on scales less than $200 h^{-1}$ kpc; thus, all the complications of the interstellar medium and small scale dynamics are ignored. Second, even to the extent that the simulation is physically accurate, the dependence of the results on cosmological parameters is unknown. Third, these results

concern *stellar mass density*, not galaxy number density. Since the galaxies in the densest regions of the simulations overmerge, to what degree the bias described here affects the brightness, rather than the number, of galaxies is unknown. (Note that the latter result would still be interesting, given that Bromley *et al.* 1998 found that early-type galaxies are fainter in dense regions than elsewhere). We plan future simulations of higher resolution to both probe variations in cosmology and to attempt to identify individual galaxies even in the denser regions of the simulation.

The general result of the simulations is that the relationship between mass and galaxies is interestingly complicated. Given the precision and volume of upcoming redshift surveys, it is possible that our understanding of the mass distribution on small scales will be limited by our ignorance of the properties of galaxy formation and of the origin of different morphological types. Hopefully, cosmological simulations such as this one can help us understand in what ways, and possibly to what degree, the galaxy distribution can differ from that of the mass.

This work was supported in part by the grants NAG5-2759, AST93-18185 and AST96-16901. MAS acknowledges the additional support of the Alfred P. Sloan Foundation, and Research Corporation. We would like to thank David N. Spergel for useful discussions.

REFERENCES

- Babul, A., & Postman, M. 1990, ApJ, 359, 280
- Balogh, M. L., Schade, D., Morris, S. L., Yee, H. K. C., Carlberg, R. G., Ellingson, E. 1998, preprint (astro-ph/9806146)
- Bromley, B. C., Press, W. H., Lin, H., & Kirshner, R. P. 1998, preprint (astro-ph/9805197)
- Cen, R. & Ostriker, J. P. 1992a, ApJ, 393, 22
- Cen, R. & Ostriker, J. P. 1992b, ApJ, 399, L113
- Cen, R. & Ostriker, J. P. 1993, ApJ, 417, 415
- Cen, R. & Ostriker, J. P. 1998a, in preparation
- Cen, R. & Ostriker, J. P. 1998b, submitted to Science (astro-ph/9806281)
- Cole, S., Aragon-Salamanca, A., Frenk, C. S., Navarro, J. F., & Zepf, S. E. 1994, MNRAS, 271, 781

- Coles, P. 1993, MNRAS, 262, 1065
- Colless, M. 1998, preprint (astro-ph/9804079)
- Davis, M., & Geller, M. J. 1976, ApJ, 208, 13
- Davis, M., Meiksin, A., Strauss, M. A., da Costa, N., & Yahil, A. 1988, ApJ, 333, L9
- Dekel, A. 1994, ARA&A, 32, 371
- Dekel, A. & Lahav, O. 1998, preprint (astro-ph/9806193)
- de Laix, A. A. & Starkman, G. 1998, ApJ, 501, 427
- Dressler, A. 1980, ApJ, 236, 351
- Fry, J. N. 1996, ApJ, 461, L65
- Fry, J. N. & Gaztañaga, E. 1993, ApJ, 413, 447
- Fukugita, M., Hogan, C. J., & Peebles, P. J. E. 1997, preprint (astro-ph/9712020)
- Giovanelli, R., Haynes, M. P., & Chincarini, G. L. 1986, ApJ, 300, 77
- Goldberg, D. M., & Strauss, M. A. 1998, ApJ, 495, 29
- Gunn, J. E., & Weinberg, D. H. 1995, in Wide-Field Spectroscopy and the Distant Universe, ed. S. J. Maddox & A. Aragón-Salamanca (Singapore: World Scientific), 3
- Guzzo, L., Strauss, M. A., Fisher, K. B., Giovanelli, R., & Haynes, M. P. 1997, ApJ, 489, 37
- Hashimoto, Y., Oemler, A., Lin H., & Tucker, D. L. 1997, preprint (astro-ph/9712319)
- Hermit, S., Santiago, B. X., Lahav, O., Strauss, M. A., Davis, M., Dressler, A., & Huchra, J. P. 1996, MNRAS, 283, 709
- Hubble, E. P. 1936, The Realm of the Nebulae (New Haven: Yale University Press)
- Huchra, J., Davis, M., Latham, D., & Tonry, J. 1983, ApJS, 52, 89
- Katz, N., Hernquist, L., & Weinberg, D. H. 1992, ApJ, 399, L109
- Katz, N., Hernquist, L., & Weinberg, D. H. 1998, preprint (astro-ph/9806257)
- Kauffmann, G., Colberg, J. M., Diaferio, A., & White S. D. M. 1998, preprint (astro-ph/9805283)

- Kauffmann, G., Nusser, A., & Steinmetz, M. 1997, MNRAS, 286, 795.
- Loveday, J., Efsthathiou, G., Maddox, S. J., & Peterson, B. A. 1996, ApJ, 468, 1
- Mann, R.G, Peacock, J.A., & Heavens, A.F. 1997, preprint (astroph/9708031)
- Oemler, A. 1974, ApJ, 194, 1
- Ostriker, J. P., & Steinhardt, P. J. 1995, Nature, 377, 600
- Postman, M., & Geller, M. 1984, ApJ, 281, 95
- Press, W. H., & Schechter, P. 1974, ApJ, 187, 425
- Santiago, B. X. & Strauss, M. A. 1992, ApJ, 387, 9
- Santiago, B. X., Strauss, M. A., Lahav, O., Davis, M., Dressler, A., & Huchra, J. P. 1995, ApJ, 446, 457
- Scherrer, R., & Weinberg, D. H. 1997, preprint (astroph/9712192)
- Sigad, Y., Eldar, A., Dekel, A., Strauss, M. A., & Yahil, A. 1998, ApJ, 495, 516
- Somerville, R. S., & Primack, J. R. 1998, preprint (astroph/9802268)
- Spergel, D. N. 1998, private communication
- Strauss, M. A., Davis, M., Yahil, A., & Huchra J. P. 1992a, ApJ, 385, 421
- Strauss, M. A., Huchra, J. P., Davis, M., Yahil, A., Fisher, K. B., & Tonry, J. 1992b, ApJS, 83, 29
- Strauss, M. A., Ostriker, J. P., & Cen, R. 1998, ApJ, 494, 20.
- Strauss, M. A., & Willick, J.A. 1995, Phys. Rep., 261, 271
- Tegmark, M., Hamilton, A. J. S., Strauss, M. A., Vogeley, M. S., & Szalay, A. S. 1998, ApJ, 499, 555
- Tegmark, M., & Peebles, P.J.E. 1998, ApJ, 500, L79
- Toomre, A. 1977, in The Evolution of Galaxies and Stellar Populations, ed. B. Tinsley & R. Larson (New Haven: Yale Univ. Obs.), 401
- Wang, Y., Spergel, D. N., & Strauss, M. A. 1998, preprint (astroph/9802231)

- Weinberg, D. H. 1995, in *Wide-Field Spectroscopy and the Distant Universe*, ed. S. J. Maddox & A. Aragón-Salamanca (Singapore: World Scientific), 129
- Whitmore, B. C., Gilmore, D. M., & Jones, C. 1993, *ApJ*, 407, 489
- Willick, J. A., & Strauss, M. A. 1998, *ApJ*, 507, in press (astro-ph/9801307)
- Young, J. S., Allen, L., Kenney, J. D. P., Lesser, A., & Rownd, B. 1996, *AJ*, 112, 1903

Table 1. Age and redshift ranges of galaxy particle quartiles of equal total mass.

Quartile	Age Range (Gyrs)	Redshift Range
Oldest	9.6 — 12.7	1.9 — ∞
Second Oldest	7.8 — 9.6	1.1 — 1.9
Second Youngest	5.7 — 7.8	0.6 — 1.1
Youngest	0 — 5.7	0 — 0.6

Table 2. Moments of total mass and galaxy mass density distributions.

Top hat radius (h^{-1} Mpc)	σ	$b \equiv \sigma_g/\sigma$	$r \equiv \langle \delta\delta_g \rangle / \sigma\sigma_g$	σ_b/σ_g	$\sigma_b/\sigma_g\sqrt{1-r^2}$
1.0	4.77	2.61	0.886	0.420	0.905
2.0	2.67	1.94	0.902	0.367	0.850
5.0	1.14	1.52	0.923	0.314	0.817
8.0	0.754	1.41	0.936	0.295	0.836
16.0	0.401	1.27	0.941	0.312	0.920
30.0	0.184	1.24	0.945	0.303	0.924

Table 3. Moments of total mass and galaxy mass density distributions for each quartile.

Top hat radius (h^{-1} Mpc)	Redshift Range	$b \equiv \sigma_g/\sigma$	$r \equiv \langle \delta\delta_g \rangle / \sigma\sigma_g$	σ_b/σ_g	$\sigma_b/\sigma_g \sqrt{1-r^2}$
1.0	1.9 — ∞	3.58	0.897	0.372	0.844
	1.1 — 1.9	3.29	0.896	0.394	0.886
	0.6 — 1.1	2.67	0.745	0.558	0.836
	0 — 0.6	2.13	0.524	0.687	0.807
30.0	1.9 — ∞	1.65	0.990	0.139	0.981
	1.1 — 1.9	1.56	0.979	0.188	0.928
	0.6 — 1.1	1.25	0.882	0.437	0.929
	0 — 0.6	0.834	0.502	0.817	0.944

Table 4. Reduction in the standard deviation $\sigma_{b,2}/\sigma$ for various choices of X_i .

X_i	$\sigma_{b,2}/\sigma_b$
Local Temperature: T	0.70
Dark Matter Velocity Dispersion: $\langle v^2 \rangle$	0.68
Velocity Shear: $\Sigma/H_0^2(1+\delta)$	0.96
Oblateness (1 h^{-1} Mpc spheres): $(\lambda_1 + \lambda_2)/2\lambda_3 - 1$	0.97
Prolateness (1 h^{-1} Mpc spheres): $2\lambda_1/(\lambda_2 + \lambda_3) - 1$	0.97

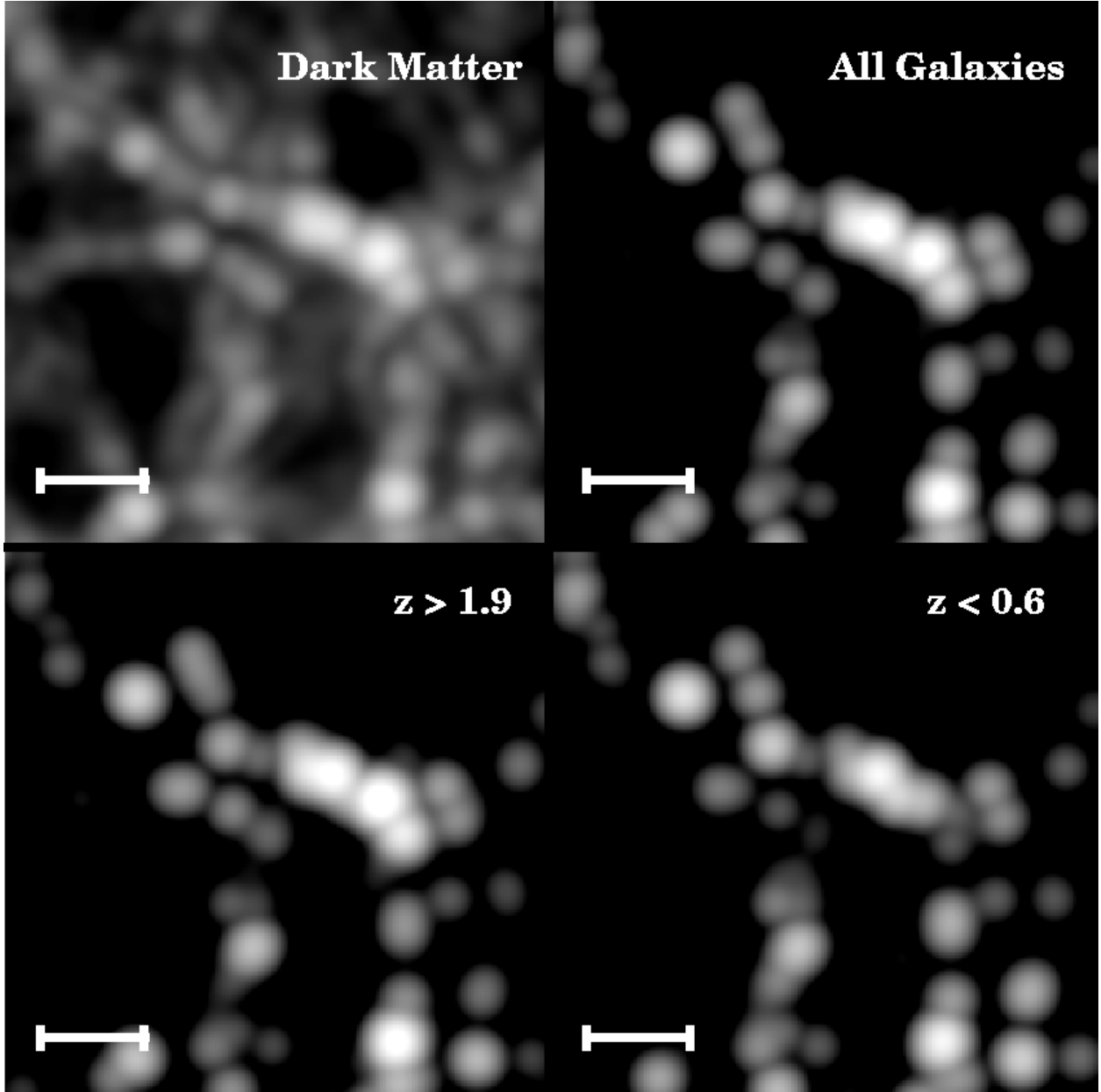


Fig. 1a.— A slice through our simulation $50 h^{-1}$ Mpc on a side (one half the total box length). As labeled, the quadrants show the fractional overdensity δ in dark matter, in the galaxies, in the young galaxies, and in the old galaxies, in clockwise order. The stretch is logarithmic and is set the same in all quadrants. The fields are smoothed with a $1 h^{-1}$ Mpc Gaussian filter. The scale bar indicates $10 h^{-1}$ Mpc. Note the large voids in the galaxy distribution and the reduction in the fraction of young galaxies in the large overdensity near the center.

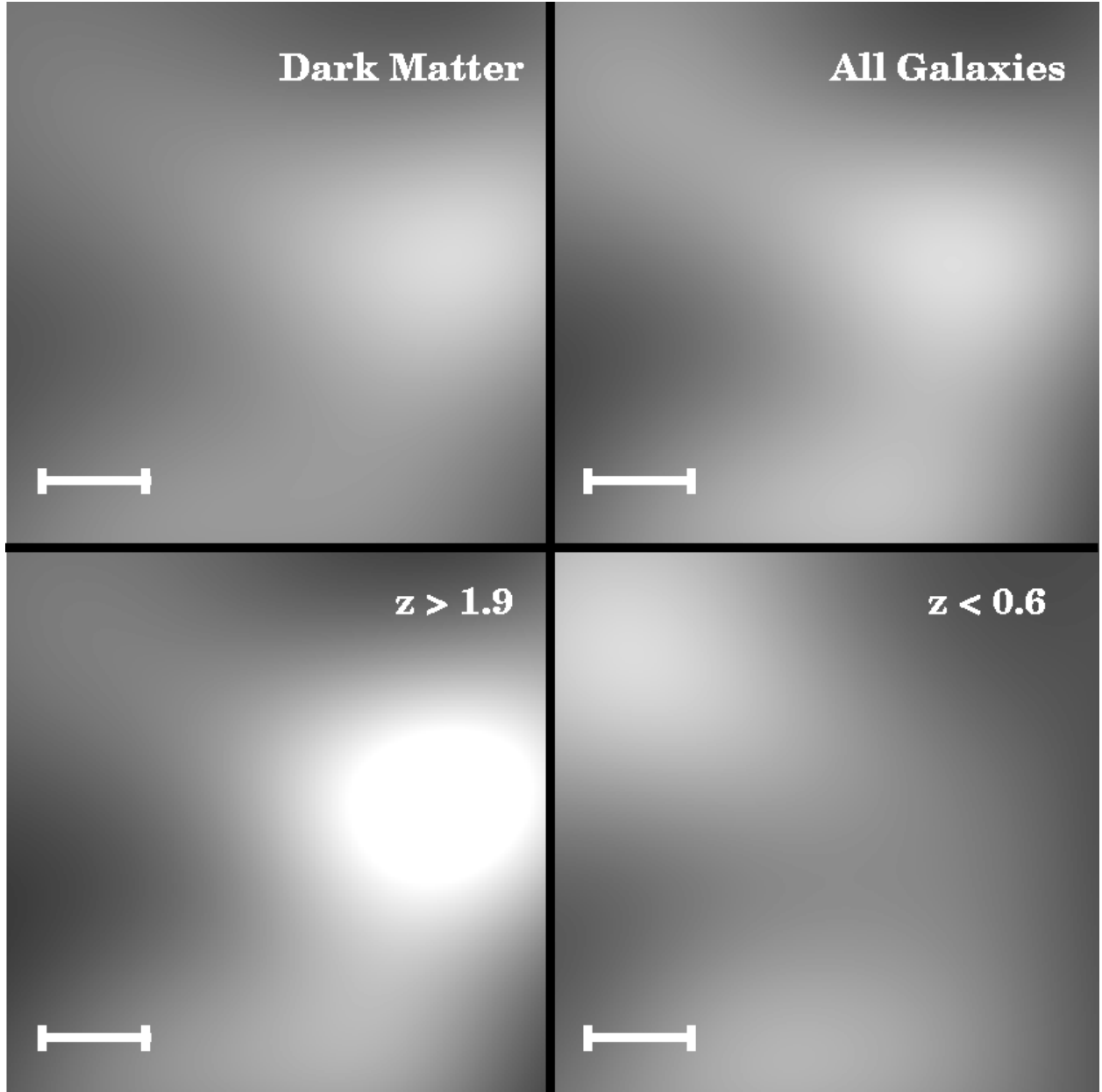


Fig. 1b.— Same as Figure 1a, now using $10 h^{-1}$ Mpc Gaussian smoothing. It is apparent now that on these scales the oldest galaxies are highly biased and that the young galaxies are poorly correlated with the mass. They appear to be overdense along the filaments but underdense in the clusters.

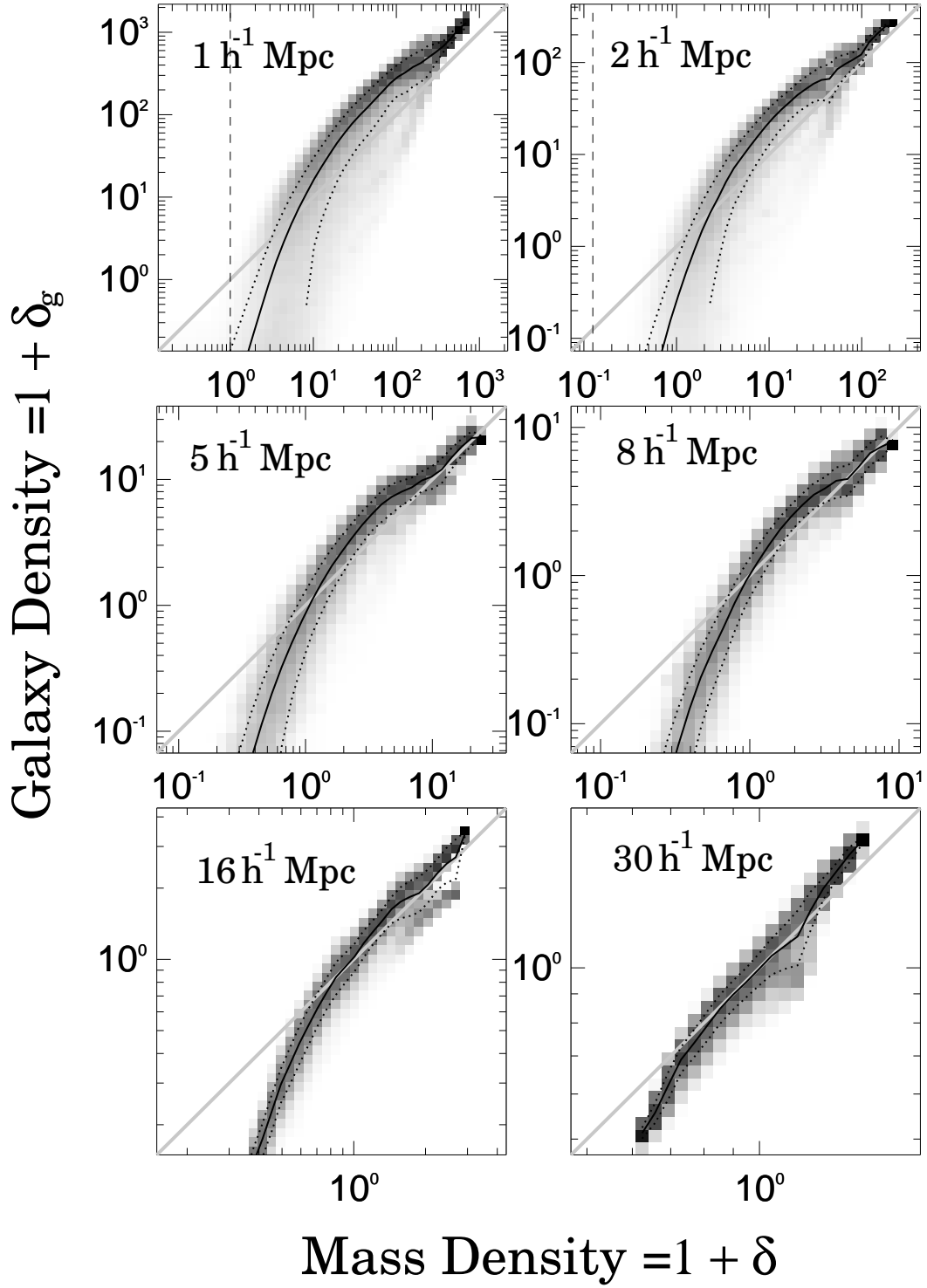


Fig. 2.— Galaxy mass density as a function of mass density for a variety of top hat smoothing radii. The shading is a logarithmic stretch of the conditional probability $P(1 + \delta_g | 1 + \delta)$; thus, each column is normalized separately. The solid black lines indicate $\langle 1 + \delta_g | 1 + \delta \rangle$; the dotted black lines indicate the 1σ deviation from the mean.

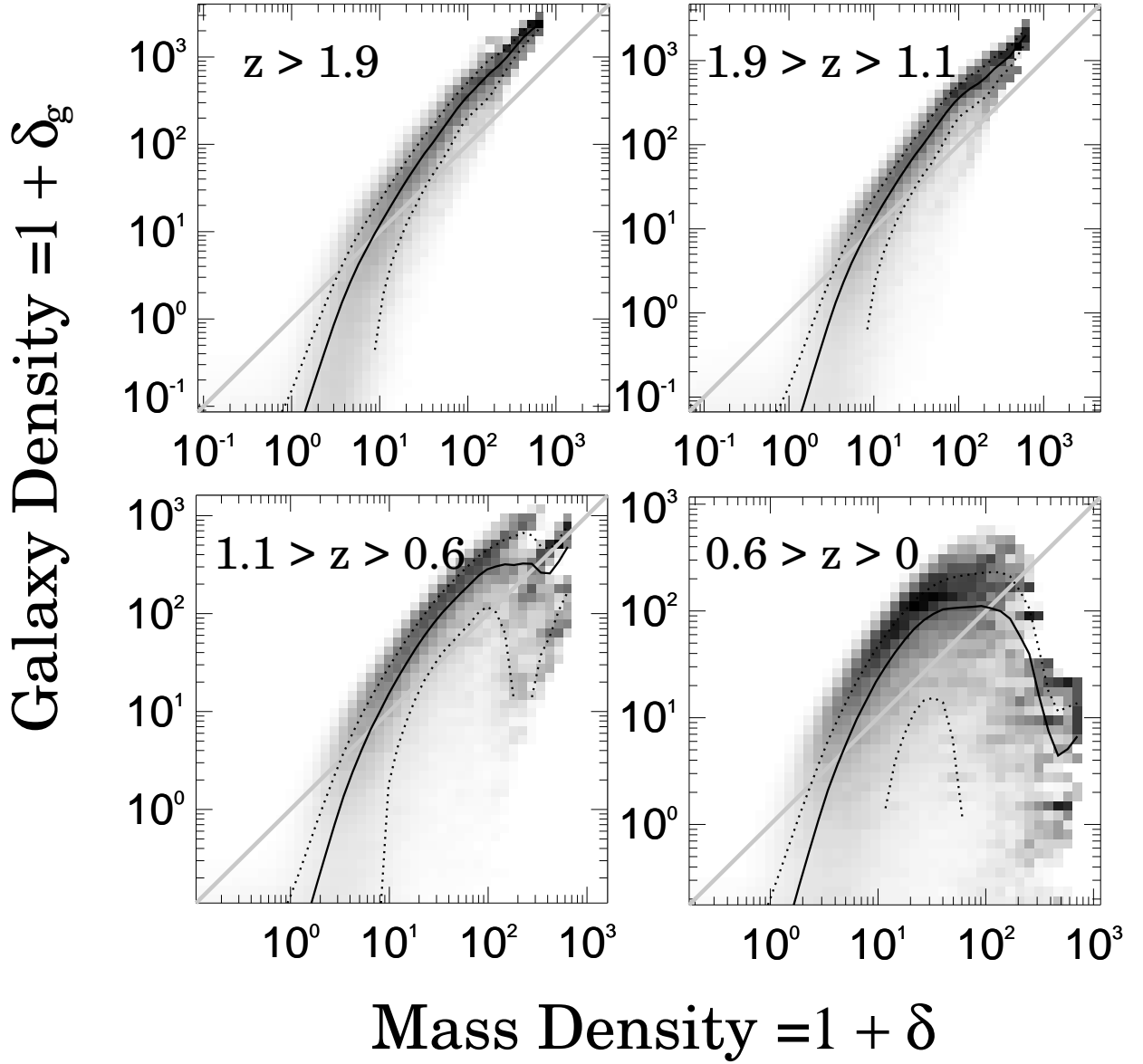


Fig. 3a.— Galaxy mass density as a function of dark matter density for each age quartile. Smoothing filter is a $1 h^{-1}$ Mpc radius top hat sphere. In each panel we list the range of formation redshifts included. The plot is of the same form as Figure 2.

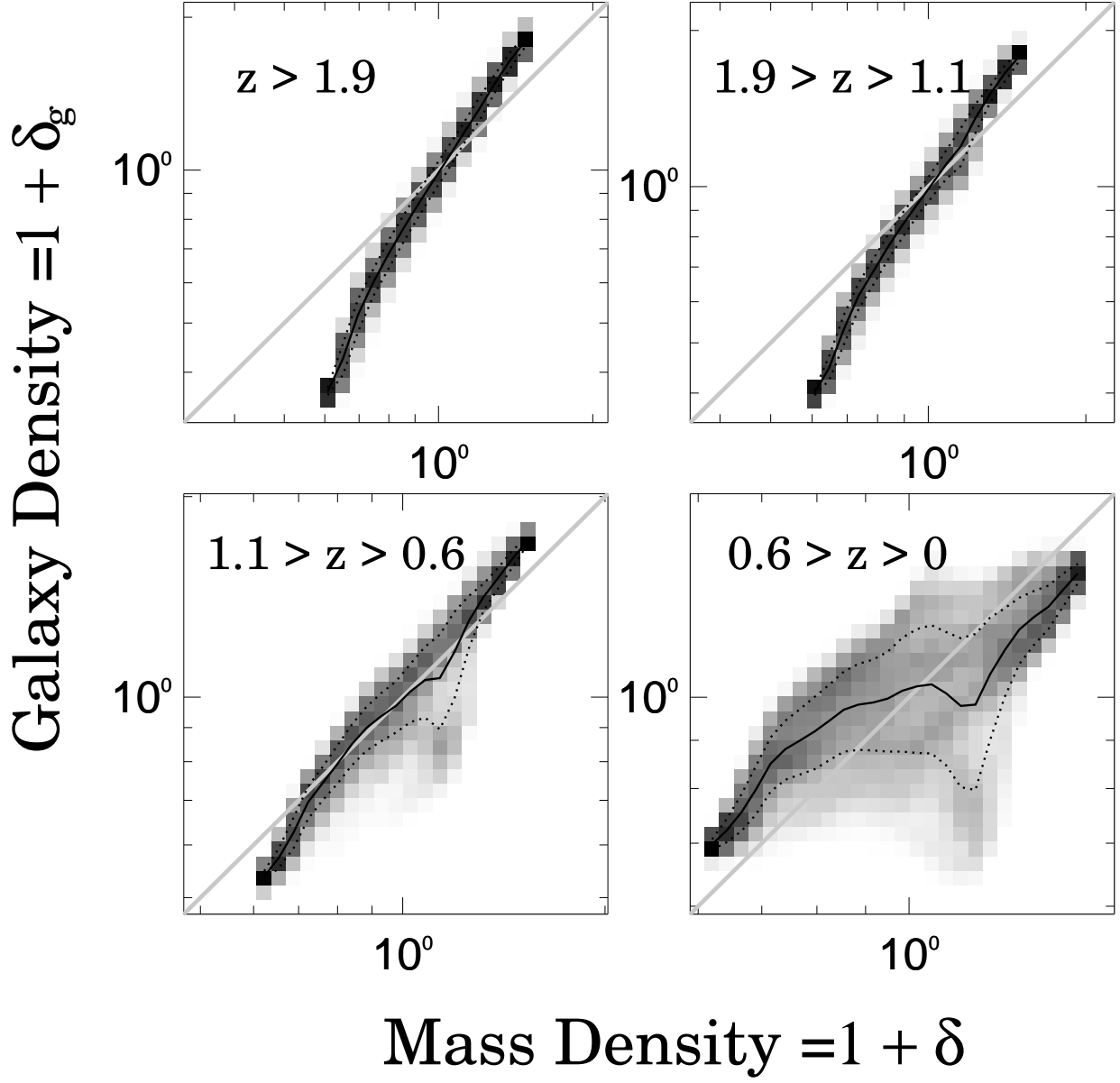


Fig. 3b.— Same as Figure 3a, with a $30 h^{-1}$ Mpc radius top hat smoothing filter.

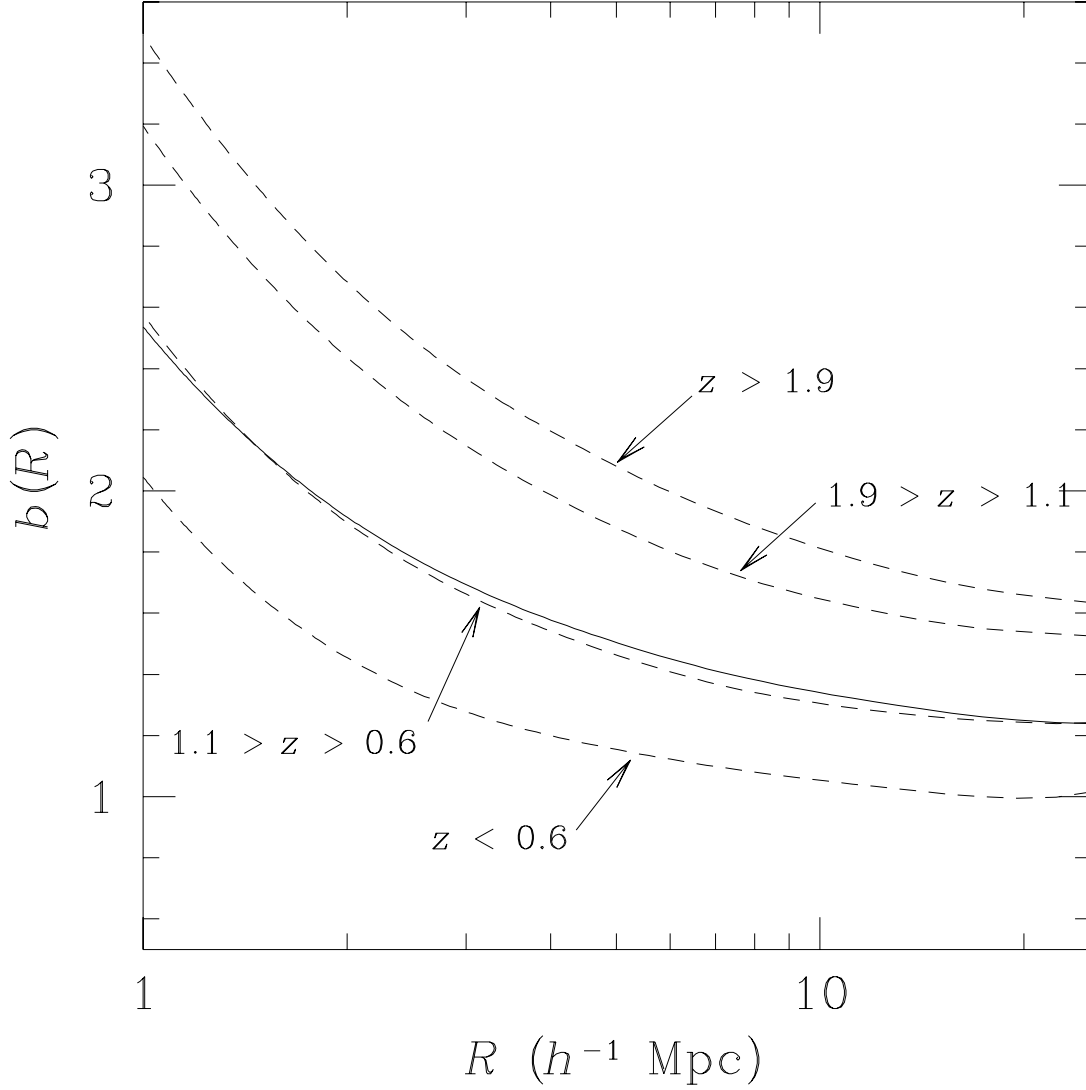


Fig. 4.— The bias $b(R) \equiv \sigma_g(R)/\sigma(R)$. The solid line indicates all the galaxies. The dashed lines indicate the age quartiles, with range of formation redshifts listed. Note the strong scale-dependence, and the fact that old galaxies are more biased than young galaxies.

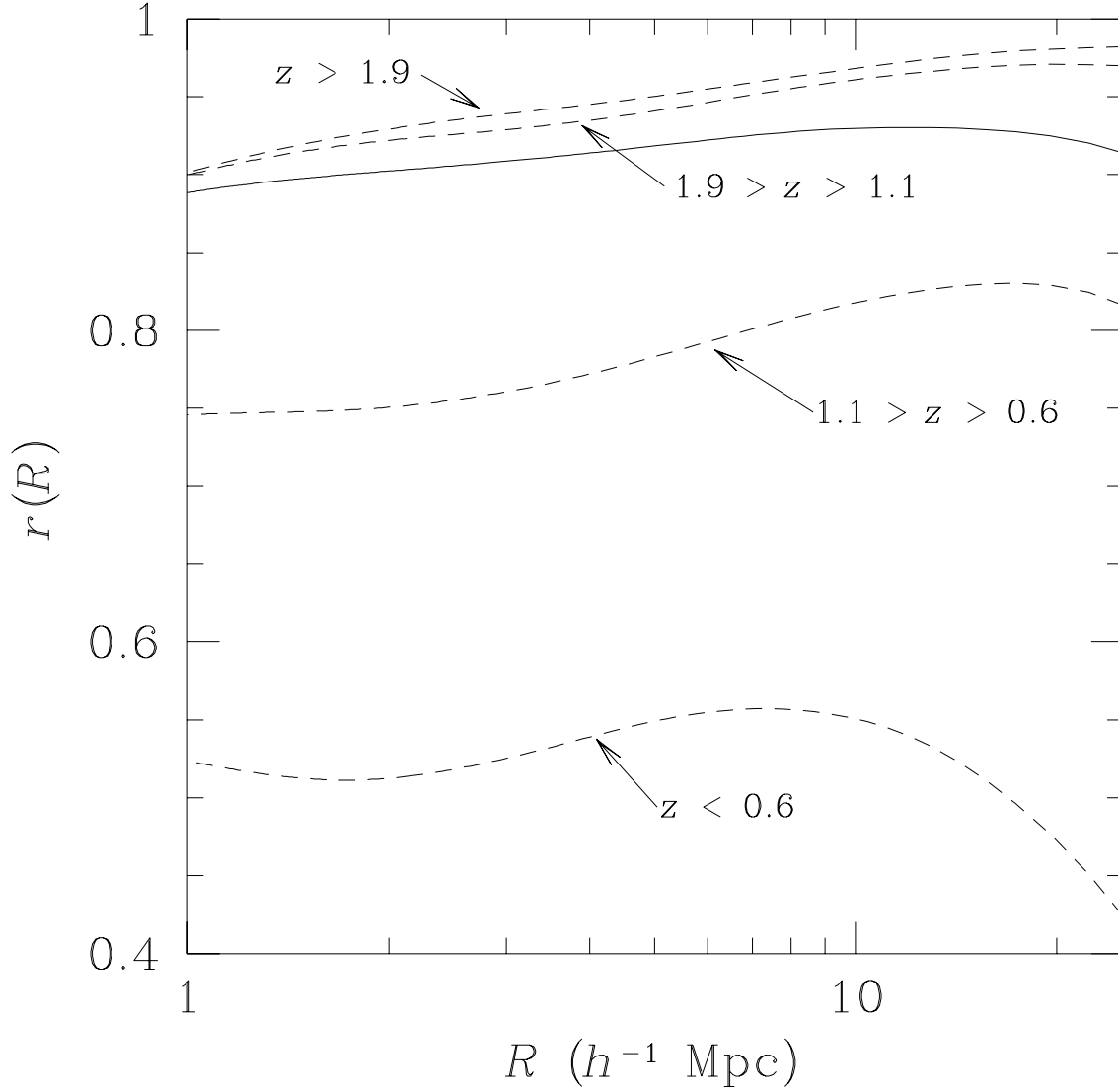


Fig. 5.— The correlation coefficient $r(R) \equiv \langle \delta_g \delta \rangle / \sigma_g(R) \sigma(R)$ as defined in the text. The lines have the same meanings as in Figure 4. The youngest galaxies are poorly correlated with the underlying mass distribution at all scales. For the oldest galaxies, the decline at small scales of the correlation coefficient is probably mainly due to the nonlinearity of $\langle \delta_g | \delta \rangle$.

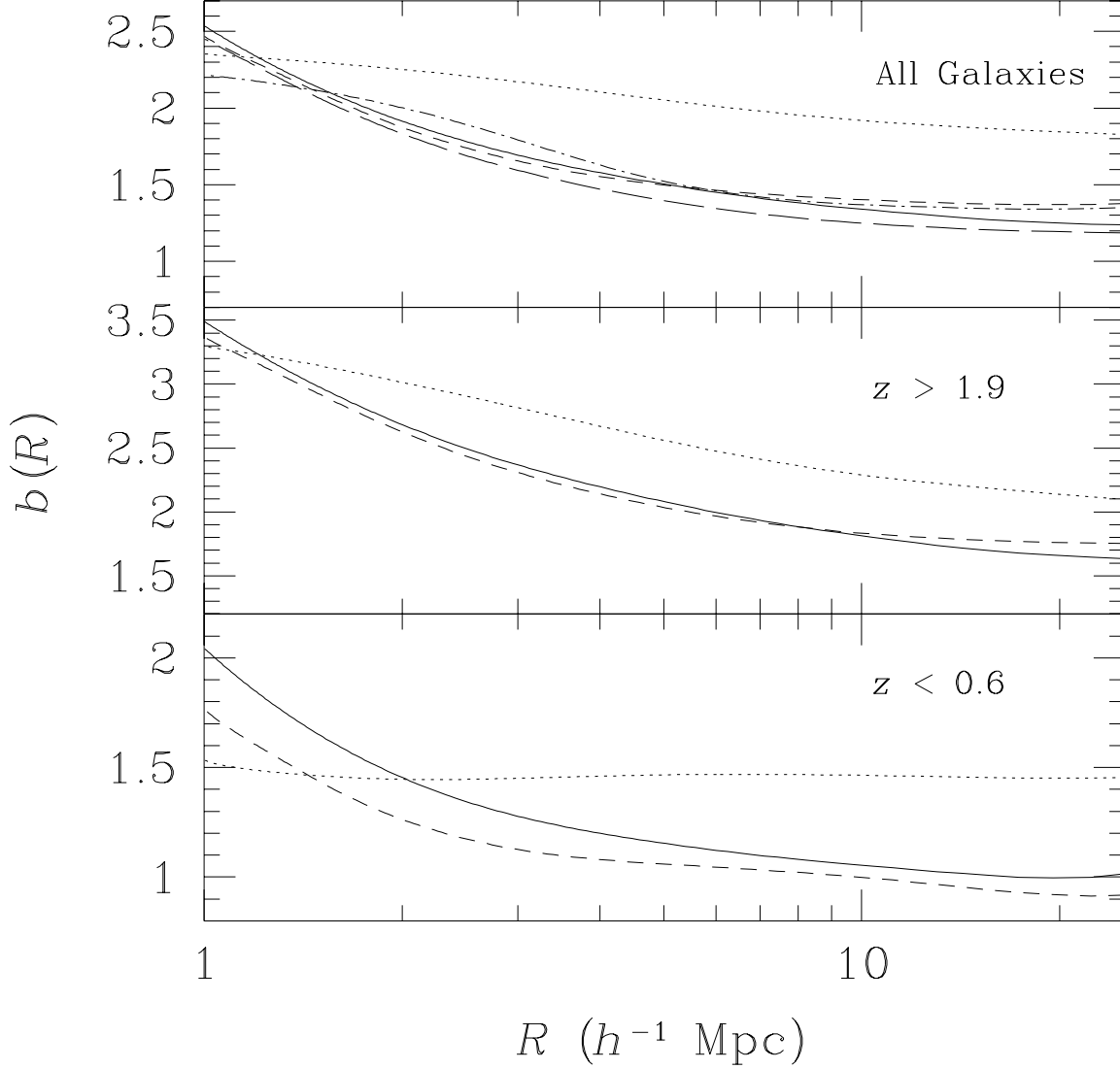


Fig. 6.— The bias $b(R)$ for various bias models compared with $b(R)$ for the galaxy particles in the simulations. As labeled, the top panel refers to all the galaxies, the middle panel to the oldest quartile of galaxies, and the bottom panel to the youngest quartile of galaxies. The solid lines are for the actual galaxy particles. The dotted lines are for a galaxy field defined by $\langle \delta_g | \delta \rangle$, with a $1 h^{-1}$ Mpc tophat smoothing. The short dashed lines are for a galaxy field defined by $\langle \delta_g | \delta, T \rangle$. The long dashed lines are for a galaxy field defined by the fit to $\langle \delta_g | \delta, T \rangle$ given in Equation 9. The dot-dashed line is for a galaxy field defined by the toy model in Equation (13), with $M' = 2.4$ and $N' = -0.4$. All the two-variable models reproduce the scale-dependence much better than does the single-variable model.

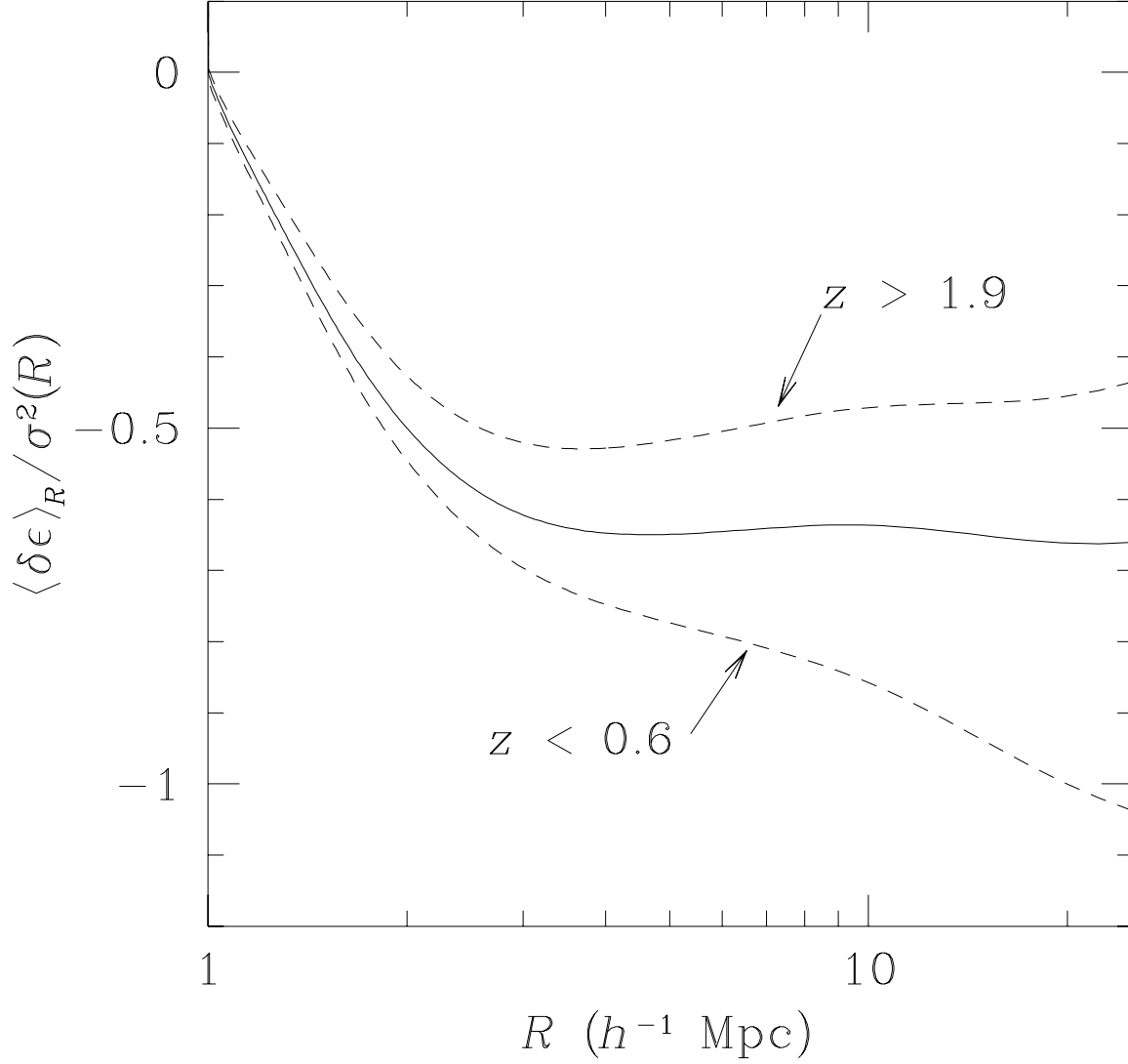


Fig. 7.— The correlations between the density field δ and the residuals $\epsilon \equiv \delta_g - \langle \delta_g | \delta \rangle$ defined on $1 \ h^{-1} \text{ Mpc}$ scales, as a function of scale. The solid curve is for all galaxies, and the dashed are for the oldest and youngest quartiles, as labeled. As explained in the text, the correlation of residuals with the large scale field is an indication that $b(R)$ will be a function of scale. Also note that the dependence is stronger for the young galaxies than for the old.

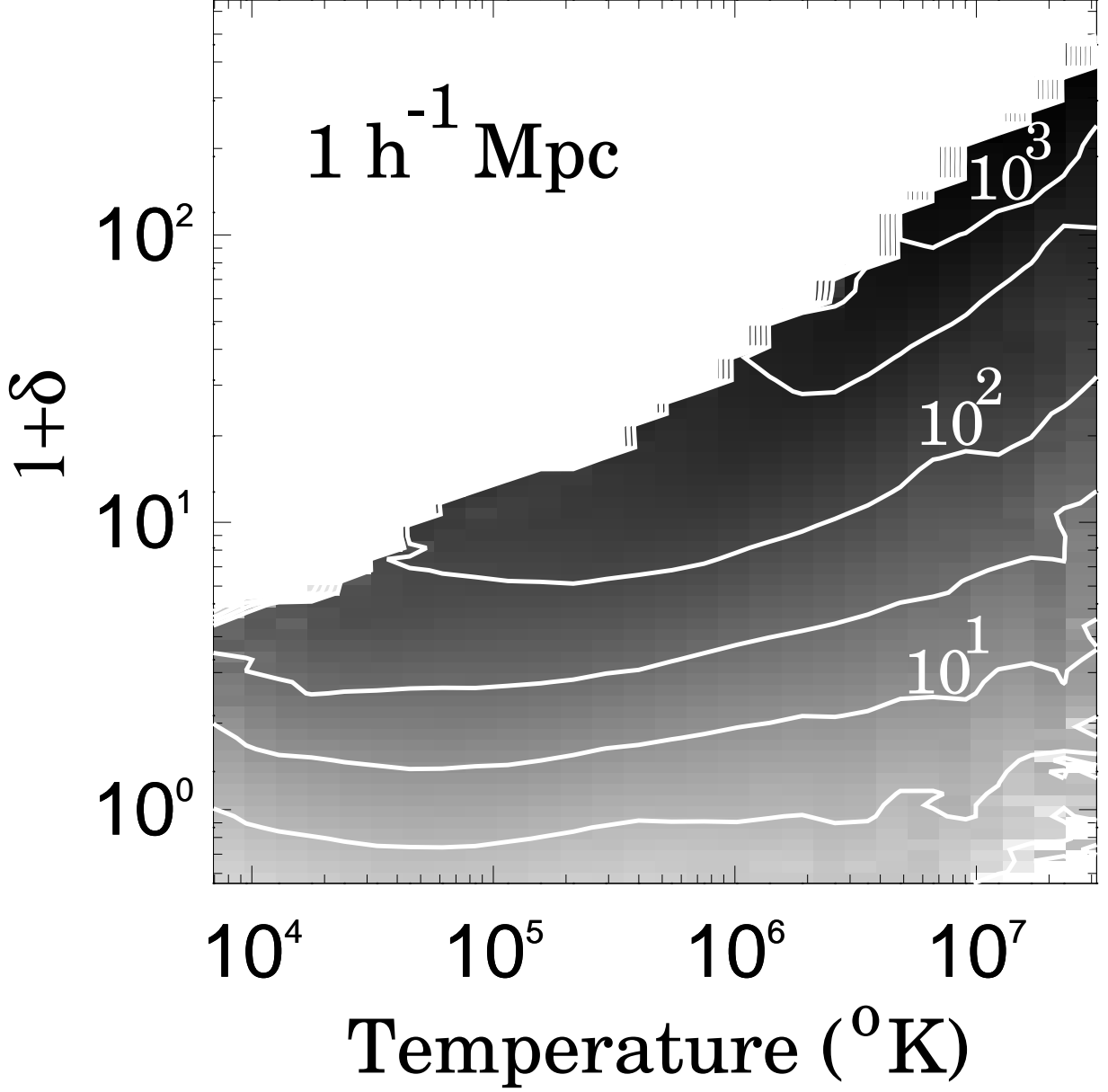


Fig. 8.— Dependence of galaxy density $1+\delta_g$ on dark matter density $1+\delta$ and temperature T , evaluated at $1 h^{-1} \text{ Mpc}$ smoothing. The greyscale is a logarithmic stretch of $1+\delta_g$; the contours are in even logarithmic intervals.

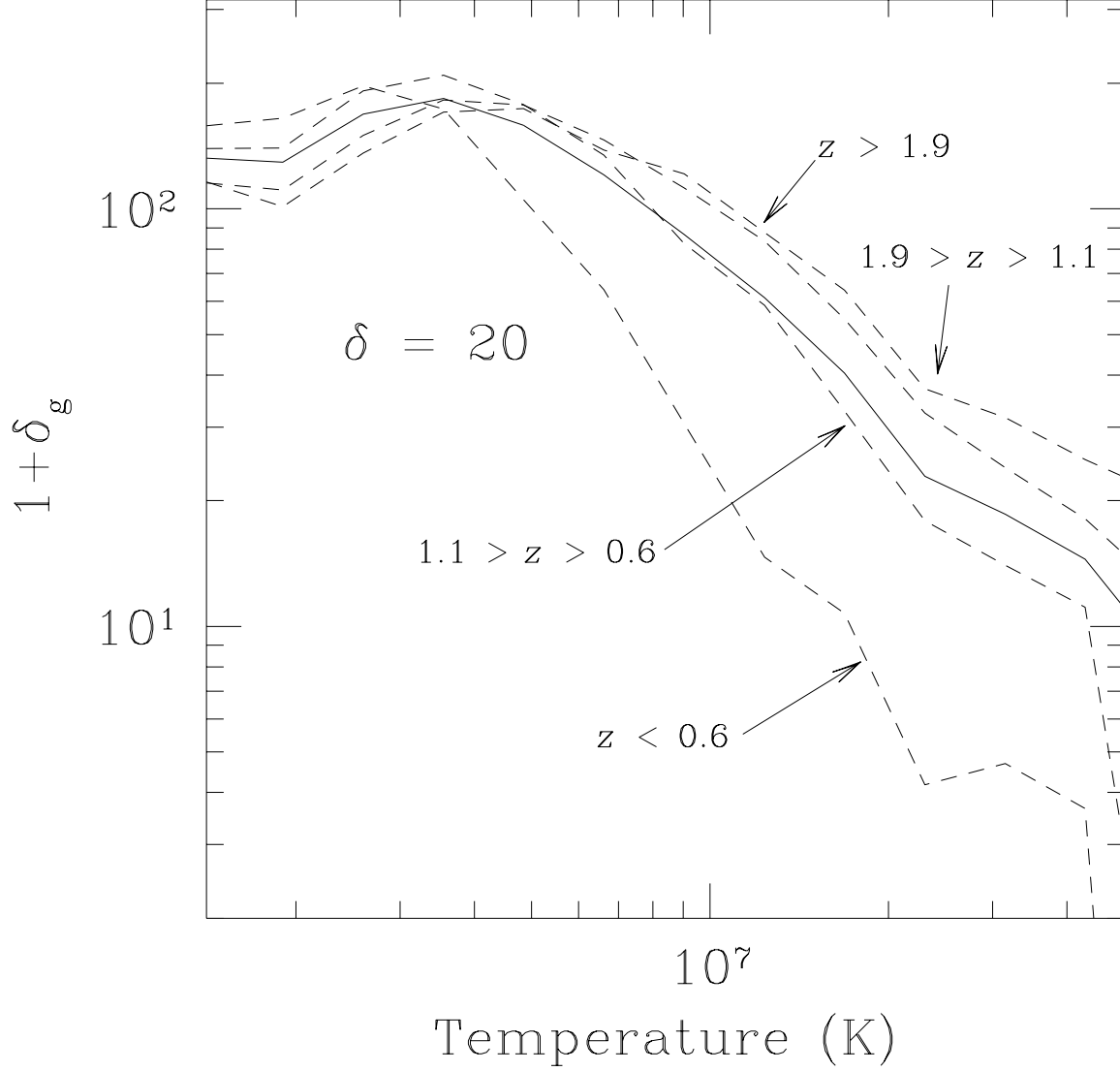


Fig. 9.— The dependence of $\rho_g/\langle\rho_g\rangle \equiv 1 + \delta_g$ on T at fixed δ for all the galaxies (solid line) and each quartile (dashed lines, as labeled). Note that $(1 + \delta_g)$ varies over an order of magnitude in this temperature range. Also, note that the young galaxies have the weakest dependence on temperature and the oldest galaxies have the strongest.

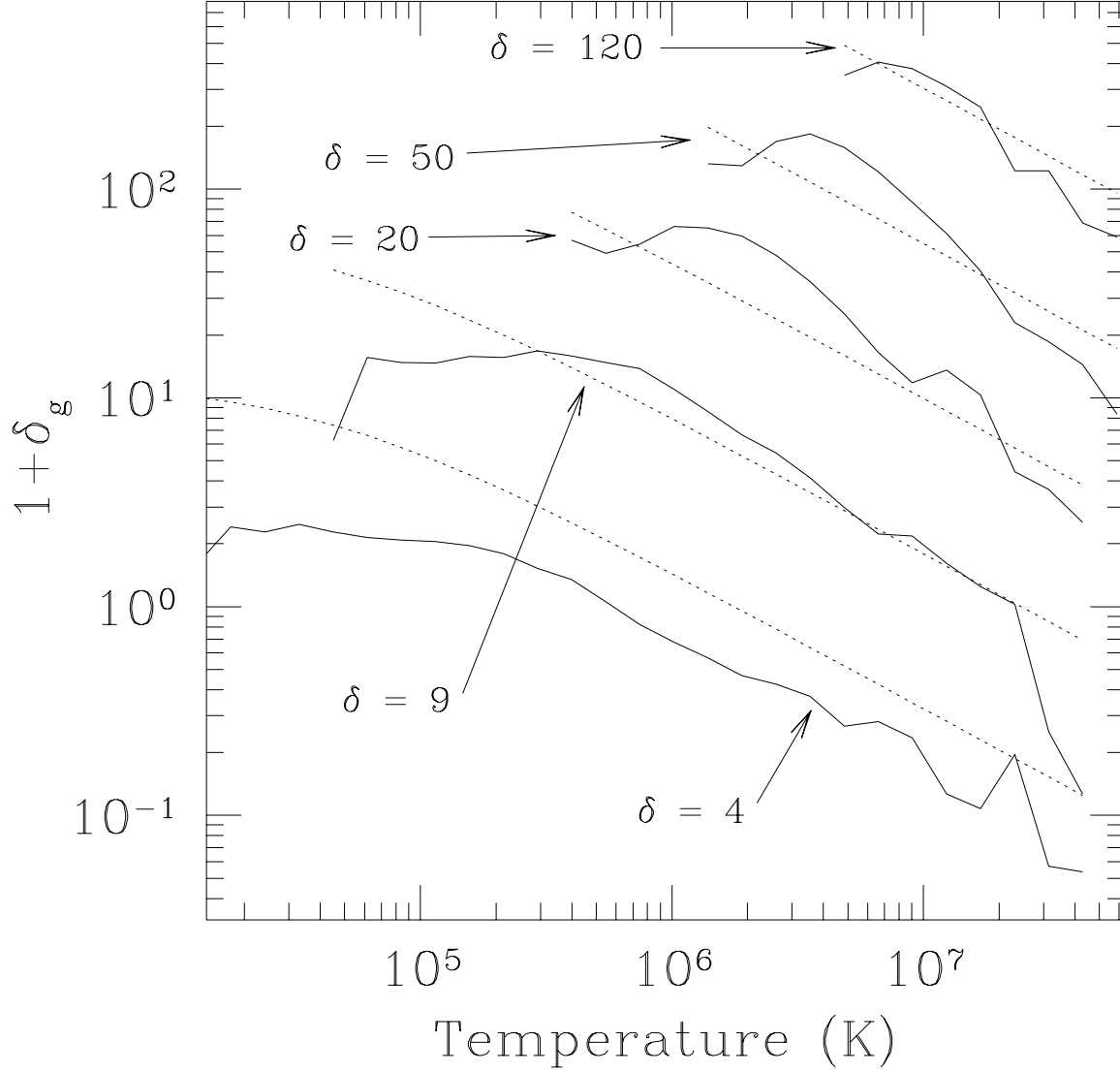


Fig. 10.— The dependence of $\rho_g/\langle\rho_g\rangle \equiv 1 + \delta_g$ on T at a series of fixed δ for all the galaxies. The solid lines are the actual dependence of the galaxies in the simulations found in Figure 8. The dotted lines are from the fit in Equation (9), with the parameters $L = 1.23$, $M = 1.9$, and $N = -0.66$.

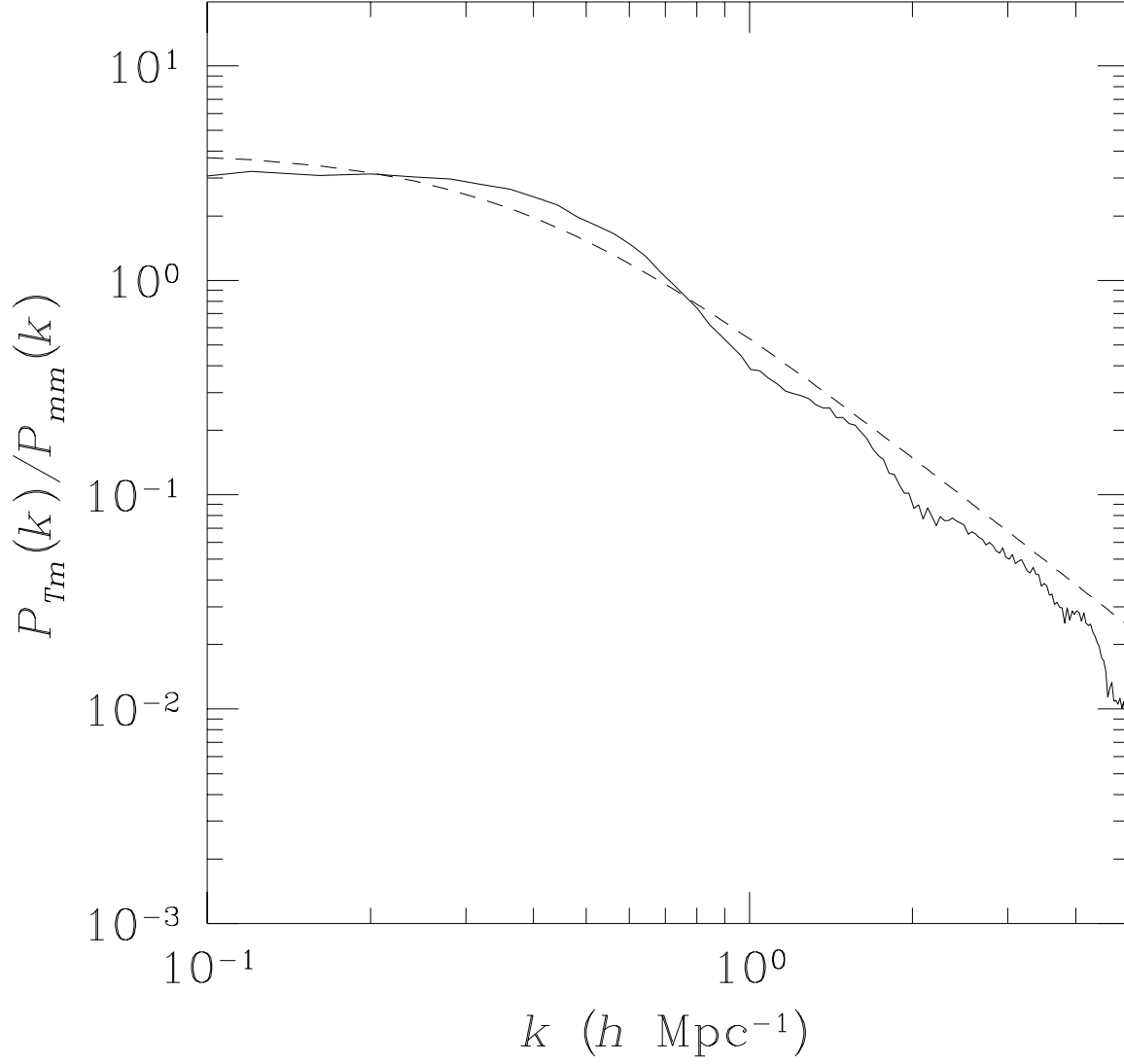


Fig. 11.— Comparison of the simple model for the temperature-density cross spectrum given in Equation 12 with the cross spectrum measured in the simulations. The solid line is from the simulations and the dashed line is the model, for $r_{nl} = 16 \text{ } h^{-1} \text{ Mpc}$.

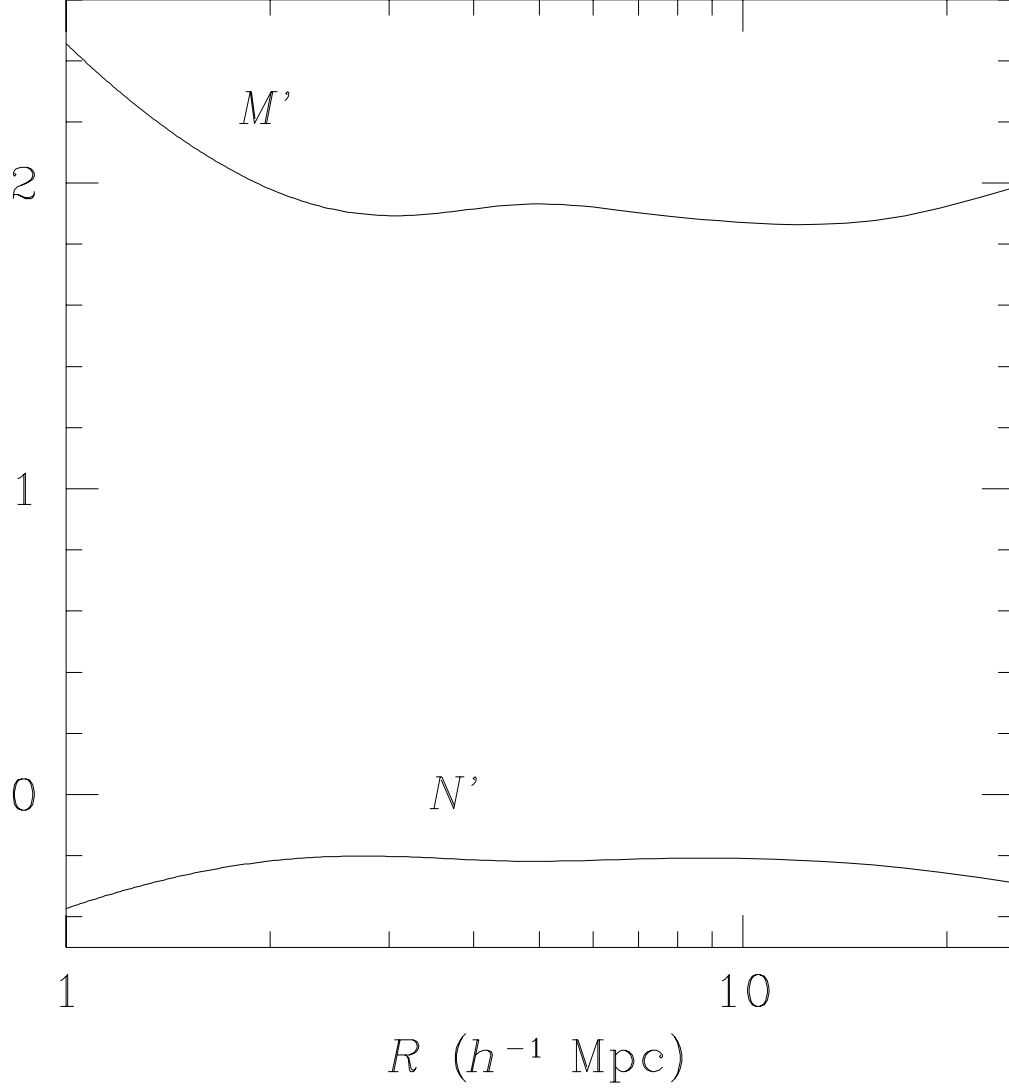


Fig. 12.— The linear parameters M' and N' of Equation (13), as a function of scale. We calculated these using a linear regression on δ and δ_T . Note the scale independence of this model, as compared to the scale dependence in the single-variable model parameter $b(R)$, shown in Figure 4.